

HIGGS BOSON PRODUCTION VIA GLUON FUSION:
SQUARK LOOPS AT NLO QCD*

MARGARETE MÜHLEITNER^{1,2} AND MICHAEL SPIRA³

¹ *CERN, Theory Division, CH-1211 Genève 23, Switzerland*

² *Laboratoire d'Annecy-Le-Vieux de Physique Théorique, LAPTH, Annecy-Le-Vieux, France*

³ *Paul Scherrer Institut, CH-5232 Villigen PSI, Switzerland*

Abstract

The loop-induced processes $gg \rightarrow h, H, A$ provide the dominant Higgs boson production mechanisms at the Tevatron and LHC in a large range of the minimal supersymmetric extension of the Standard Model. For squark masses below ~ 400 GeV squark loop contributions become important in addition to the top and bottom quark loops. The next-to-leading order QCD corrections to the squark contributions of these processes are determined including the full squark and Higgs mass dependences. They turn out to be large and thus important for the Tevatron and LHC experiments. Squark mass effects of the K factors can be of $\mathcal{O}(20\%)$. In addition we derive the QCD corrections to the squark contributions of the rare photonic Higgs decays $h, H \rightarrow \gamma\gamma$, which play a role for the Higgs searches at the LHC.

*Supported in part by the Swiss Bundesamt für Bildung und Wissenschaft.

1 Introduction

Higgs boson [1] searches belong to the major endeavors at present and future colliders within the Standard Model (SM) and its minimal supersymmetric extension (MSSM). In the MSSM two isospin Higgs doublets are introduced in order to generate masses of up- and down-type fermions [2]. After electroweak symmetry breaking three of the eight degrees of freedom are absorbed by the Z and W gauge bosons, leaving five states as elementary Higgs particles. These consist of two CP-even neutral (scalar) particles h, H , one CP-odd neutral (pseudoscalar) particle A and two charged bosons H^\pm . At leading order the MSSM Higgs sector is fixed by two independent input parameters which are usually chosen as the pseudoscalar Higgs mass M_A and $\text{tg}\beta = v_2/v_1$, the ratio of the two vacuum expectation values. Including the one-loop and dominant two-loop corrections the upper bound of the light scalar Higgs mass is $M_h \lesssim 140$ GeV [3]. The couplings of the various neutral Higgs bosons to fermions and gauge bosons, normalized to the SM Higgs couplings, are listed in Table 1, where the angle α denotes the mixing angle of the scalar Higgs bosons h, H . An important property of the bottom Yukawa couplings is their enhancement for large values of $\text{tg}\beta$, while the top Yukawa couplings are suppressed for large $\text{tg}\beta$ [4].

ϕ		g_u^ϕ	g_d^ϕ	g_V^ϕ
SM	H	1	1	1
MSSM	h	$\cos \alpha / \sin \beta$	$-\sin \alpha / \cos \beta$	$\sin(\beta - \alpha)$
	H	$\sin \alpha / \sin \beta$	$\cos \alpha / \cos \beta$	$\cos(\beta - \alpha)$
	A	$1/\text{tg}\beta$	$\text{tg}\beta$	0

Table 1: *Higgs couplings in the MSSM to fermions and gauge bosons [$V = W, Z$] relative to the SM couplings.*

For this work we need the Higgs couplings to stop and sbottom squarks in addition. The scalar superpartners $\tilde{f}_{L,R}$ of the left- and right-handed fermion components mix with each other. The mass eigenstates $\tilde{f}_{1,2}$ of the sfermions are related to the current eigenstates $\tilde{f}_{L,R}$ by mixing angles θ_f ,

$$\begin{aligned}\tilde{f}_1 &= \tilde{f}_L \cos \theta_f + \tilde{f}_R \sin \theta_f \\ \tilde{f}_2 &= -\tilde{f}_L \sin \theta_f + \tilde{f}_R \cos \theta_f.\end{aligned}\tag{1}$$

The mass matrix of the sfermions in the left-right-basis is given by [5]¹

$$\mathcal{M}_{\tilde{f}} = \begin{bmatrix} M_{\tilde{f}_L}^2 + m_f^2 & m_f(A_f - \mu r_f) \\ m_f(A_f - \mu r_f) & M_{\tilde{f}_R}^2 + m_f^2 \end{bmatrix},\tag{2}$$

¹For simplicity, the D -terms have been absorbed in the sfermion-mass parameters $M_{\tilde{f}_{L/R}}^2$.

with the parameters $r_d = 1/r_u = \text{tg}\beta$ for down- and up-type fermions. The parameters A_f denote the trilinear scalar couplings of the soft supersymmetry breaking part of the Lagrangian, μ the Higgsino mass parameter and m_f the fermion mass. The mixing angles acquire the form

$$\sin 2\theta_f = \frac{2m_f(A_f - \mu r_f)}{M_{\tilde{f}_1}^2 - M_{\tilde{f}_2}^2} \quad , \quad \cos 2\theta_f = \frac{M_{\tilde{f}_L}^2 - M_{\tilde{f}_R}^2}{M_{\tilde{f}_1}^2 - M_{\tilde{f}_2}^2} \quad , \quad (3)$$

and the masses of the squark mass eigenstates are given by

$$M_{\tilde{f}_{1,2}}^2 = m_f^2 + \frac{1}{2} \left[M_{\tilde{f}_L}^2 + M_{\tilde{f}_R}^2 \mp \sqrt{(M_{\tilde{f}_L}^2 - M_{\tilde{f}_R}^2)^2 + 4m_f^2(A_f - \mu r_f)^2} \right] . \quad (4)$$

Since the mixing angles are proportional to the masses of the ordinary fermions, mixing effects are only important for the third-generation sfermions. The neutral Higgs couplings to sfermions read [6]

$$\begin{aligned} g_{\tilde{f}_L \tilde{f}_L}^\phi &= m_f^2 g_1^\phi + M_Z^2 (I_{3f} - e_f \sin^2 \theta_W) g_2^\phi \\ g_{\tilde{f}_R \tilde{f}_R}^\phi &= m_f^2 g_1^\phi + M_Z^2 e_f \sin^2 \theta_W g_2^\phi \\ g_{\tilde{f}_L \tilde{f}_R}^\phi &= -\frac{m_f}{2} (\mu g_3^\phi - A_f g_4^\phi) , \end{aligned} \quad (5)$$

with the couplings g_i^ϕ listed in Table 2. I_{3f} denotes the third component of the electroweak isospin, e_f the electric charge of the fermion f , θ_W the Weinberg angle and M_Z the Z -boson mass. All these couplings have to be rotated to the mass eigenstates by the mixing angle θ_f .

\tilde{f}	ϕ	g_1^ϕ	g_2^ϕ	g_3^ϕ	g_4^ϕ
\tilde{u}	h	$\cos \alpha / \sin \beta$	$-\sin(\alpha + \beta)$	$-\sin \alpha / \sin \beta$	$\cos \alpha / \sin \beta$
	H	$\sin \alpha / \sin \beta$	$\cos(\alpha + \beta)$	$\cos \alpha / \sin \beta$	$\sin \alpha / \sin \beta$
	A	0	0	-1	$1/\text{tg}\beta$
\tilde{d}	h	$-\sin \alpha / \cos \beta$	$-\sin(\alpha + \beta)$	$\cos \alpha / \cos \beta$	$-\sin \alpha / \cos \beta$
	H	$\cos \alpha / \cos \beta$	$\cos(\alpha + \beta)$	$\sin \alpha / \cos \beta$	$\cos \alpha / \cos \beta$
	A	0	0	-1	$\text{tg}\beta$

Table 2: *Coefficients of the neutral MSSM Higgs couplings to up- and down-type sfermion pairs.*

At hadron colliders as the Tevatron and LHC neutral Higgs bosons are copiously produced by the gluon fusion processes $gg \rightarrow h/H/A$, which are mediated by top and

bottom quark loops as well as stop and sbottom loops in the MSSM (see Fig. 1). Due to the large size of the top Yukawa couplings gluon fusion comprises the dominant Higgs boson production mechanism for small and moderate $\text{tg}\beta$. For large $\text{tg}\beta$ the leading role is taken over by Higgs radiation off bottom quarks due to the strongly enhanced bottom Yukawa couplings [7].

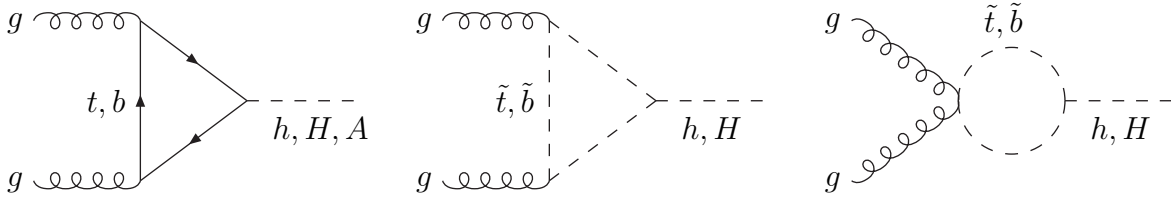


Figure 1: *MSSM Higgs boson production via gluon fusion mediated by top- and bottom quark as well as stop and sbottom loops at leading order.*

The QCD corrections to the top and bottom quark loops are known since a long time including the full Higgs and quark mass dependences [8]. They increase the cross sections by up to about 100%. The limit of very heavy top quarks provides an approximation within $\sim 20 - 30\%$ for $\text{tg}\beta \lesssim 5$ [9]. In this limit the next-to-leading order (NLO) QCD corrections have been calculated before [10] and later the next-to-next-to-leading order (NNLO) QCD corrections [11]. The NNLO corrections lead to a further moderate increase of the cross section by $\sim 20 - 30\%$, so that the dominant part are the NLO contributions. Very recently an estimate of the next-to-next-to-next-to-leading order (NNNLO) effects has been obtained [12] indicating improved perturbative convergence. A full massive NNLO calculation is not available so far, so that the NNLO results can only be used for small and moderate $\text{tg}\beta$. On the other hand the NLO corrections to the squark loops are only known in the limit of heavy squarks [13]. Moreover, the full SUSY-QCD corrections have been obtained recently for heavy SUSY particle masses [14]. NLO computations for the last two contributions including the full mass dependences are missing so far. This work presents the pure QCD corrections to the squark loops including the full squark and Higgs mass dependences as a first step towards a full NLO SUSY-QCD calculation.

The reverse processes, gluonic Higgs decays, play a role for the decay profiles of the Higgs particles. Their partial widths can be measured at a future linear e^+e^- collider with energy up to about 1 TeV [15]. The gluonic branching ratios can reach a level of $\mathcal{O}(10\%)$ in some regions of the MSSM parameter space [4,7,16]. Analogously to the gluon fusion processes the QCD corrections to the top and bottom quark loops have been calculated including the full quark and Higgs mass dependences [8]. The NLO corrections in the limit of very heavy top quarks can be found in [10,17]. This limit provides a reasonable approximation for small and moderate values of $\text{tg}\beta$. The NNLO QCD corrections are known for very heavy top quarks, too [18]. Very recently, even the NNNLO QCD corrections have been obtained in the heavy top mass limit [19]. While the NLO corrections

enhance the partial decay width by up to about 70%, the NNLO corrections turn out to be of moderate size $\mathcal{O}(20\%)$ supplemented by the NNNLO corrections in the per cent range. The quark mass effects at NNLO and beyond are unknown. The SUSY–QCD corrections to the gluonic decay mode are identical to the gluon fusion process. The full mass dependences of the NLO SUSY–QCD corrections are unknown. This work provides a first step towards this aim by determining the pure QCD corrections to the squark loops.

A subsample of the diagrams describing the Higgs couplings to gluons determines the Higgs couplings to a pair of photons. Since at NLO there is no gluon radiation, the LO and NLO results for the photonic Higgs couplings are valid for the Higgs decays into photons, which are important Higgs decay modes for the Higgs search at the LHC. Moreover, they determine Higgs boson production at a future linear photon collider, a satellite mode of a linear e^+e^- collider built up by Compton back-scattered laser light off the e^- beams [20,21]. The NLO QCD corrections to the quark loops are known in the limit of a very heavy top quark [22,23] as well as in the fully massive case [22], while the NNLO [24] and NLO SUSY–QCD [25] corrections are only known for very heavy top and SUSY-particle masses. The results presented in this paper comprise a first step towards a full massive SUSY–QCD calculation at NLO by means of the QCD corrections to the squark loops.

This paper is organized as follows. In Section 2 we describe the NLO QCD calculation of the squark loop contributions to the photonic and gluonic MSSM Higgs couplings and present the results. Section 3 summarizes and concludes.

2 NLO QCD Corrections

In order to compute the pure QCD corrections to the squark loops we need a modification of the MSSM interaction Lagrangian allowing to separate gluon and gluino exchange contributions in a renormalizeable way. This is achieved by starting from the basic Lagrangian²

$$\begin{aligned} \mathcal{L} = & -\frac{1}{4}G^{a\mu\nu}G_{\mu\nu}^a - \frac{1}{4}F^{\mu\nu}F_{\mu\nu} + \frac{1}{2}\left[(\partial_\mu\mathcal{H})^2 - M_{\mathcal{H}}^2\mathcal{H}^2\right] \\ & + \sum_{\tilde{Q}}\left[\bar{\tilde{Q}}(i\not{D} - m_{\tilde{Q}})Q - g_{\tilde{Q}}^{\mathcal{H}}\frac{m_{\tilde{Q}}}{v}\bar{\tilde{Q}}Q\mathcal{H}\right] + \sum_{\tilde{Q}}\left[|D_\mu\tilde{Q}|^2 - m_{\tilde{Q}}^2|\tilde{Q}|^2 - g_{\tilde{Q}}^{\mathcal{H}}\frac{m_{\tilde{Q}}^2}{v}|\tilde{Q}|^2\mathcal{H}\right] \end{aligned} \quad (6)$$

with the covariant derivative $D_\mu = \partial_\mu + ig_s G_\mu^a T^a + ieA_\mu \mathcal{Q}$. Here $G_{\mu\nu}^a$ denotes the gluon field strength tensor and G_μ^a the gluon field accompanied by the color $SU(3)$ generators T^a ($a = 1, \dots, 8$), while $F_{\mu\nu}$ is the photon field strength tensor and A_μ the photon field associated by the electric charge operator \mathcal{Q} . The Higgs field \mathcal{H} represents generically either the light scalar h or the heavy scalar H Higgs boson of the MSSM³. In this work the couplings $g_{\tilde{Q}}^{\mathcal{H}}$ and $g_{\tilde{Q}}^{\mathcal{H}}$ are not renormalized, thus leading to a renormalizeable model

²Quartic selfinteractions among the squarks are not taken into account in this work.

³Since there are no squark loop contributions to the pseudoscalar Higgs boson couplings to photons and gluons at leading order (LO), in this paper we will only deal with the scalar Higgs bosons h, H .

with strongly interacting scalars \tilde{Q} . Only if gluino exchange contributions were taken into account, the full MSSM renormalization would have to be performed. It should be noted that the gluino contributions can be separated from the QCD corrections induced by light particles due to the gluino mass. Gluino corrections are expected to be small [14].

The numerical results in this work will be presented for the gluophobic Higgs scenario [26], which develops strong interference effects between quarks and squarks. It is defined by the following choices of the MSSM parameters [$m_t = 174.3$ GeV],

$$\begin{aligned}
M_{SUSY} &= 350 \text{ GeV} \\
\mu = M_2 &= 300 \text{ GeV} \\
X_t &= -770 \text{ GeV} \\
A_b &= A_t \\
m_{\tilde{g}} &= 500 \text{ GeV},
\end{aligned} \tag{7}$$

where $X_t = A_t - \mu/\text{tg}\beta$. We have used the program HDECAY [16] for the numerical determination of the SUSY particle masses and couplings. In this scenario the squark masses amount to

$$\begin{aligned}
\text{tg}\beta = 3 : \quad & m_{\tilde{t}_1} = 156 \text{ GeV} \\
& m_{\tilde{t}_2} = 517 \text{ GeV} \\
& m_{\tilde{b}_1} = 346 \text{ GeV} \\
& m_{\tilde{b}_2} = 358 \text{ GeV} \\
\text{tg}\beta = 30 : \quad & m_{\tilde{t}_1} = 155 \text{ GeV} \\
& m_{\tilde{t}_2} = 516 \text{ GeV} \\
& m_{\tilde{b}_1} = 314 \text{ GeV} \\
& m_{\tilde{b}_2} = 388 \text{ GeV}.
\end{aligned} \tag{8}$$

The gluophobic scenario maximizes the destructive interference effects between top and stop loop contributions to the light scalar Higgs coupling to gluons. The results of this work look similar, whenever the squark masses turn out to be of the order of the top mass, or the Higgs mass reaches values beyond the corresponding squark-antisquark threshold.

2.1 Scalar Higgs Boson Couplings to Photons

At leading order (LO) the photonic MSSM Higgs couplings are mediated by top and bottom quark loops as well as W loops for the scalar Higgs particles h, H . If the stop and sbottom masses range below ~ 400 GeV, there are significant contributions from squark loops, too (see Fig. 2). The LO photonic decay widths are given by [7,8,27]

$$\begin{aligned}
\Gamma_{LO}(h/H \rightarrow \gamma\gamma) &= \frac{G_F \alpha^2 M_{h/H}^3}{36\sqrt{2}\pi^3} \left| g_W^{h/H} A_W^{h/H}(\tau_W) + \sum_f N_{cf} e_f^2 g_f^{h/H} A_f^{h/H}(\tau_f) \right. \\
&\quad \left. + \sum_{\tilde{f}} N_{c\tilde{f}} e_{\tilde{f}}^2 g_{\tilde{f}}^{h/H} A_{\tilde{f}}^{h/H}(\tau_{\tilde{f}}) \right|^2
\end{aligned} \tag{9}$$

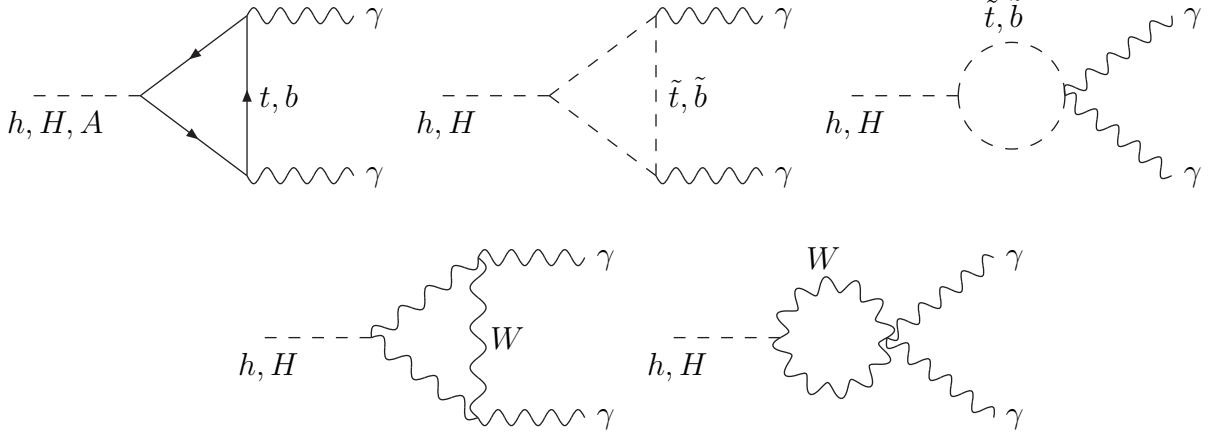


Figure 2: *MSSM Higgs boson couplings to photon pairs mediated by top- and bottom quark, stop and sbottom as well as W boson loops at leading order.*

$$\begin{aligned}
A_W^{h/H}(\tau) &= -[2 + 3\tau + 3\tau(2 - \tau)f(\tau)] \\
A_f^{h/H}(\tau) &= 2\tau[1 + (1 - \tau)f(\tau)] \\
A_{\tilde{f}}^{h/H}(\tau) &= -\tau[1 - \tau f(\tau)] \\
f(\tau) &= \begin{cases} \arcsin^2 \frac{1}{\sqrt{\tau}} & \tau \geq 1 \\ -\frac{1}{4} \left[\log \frac{1 + \sqrt{1 - \tau}}{1 - \sqrt{1 - \tau}} - i\pi \right]^2 & \tau < 1 \end{cases},
\end{aligned}$$

where we neglected contributions from charginos, charged Higgs bosons and the charged sleptons. The full expressions can be found e.g. in [7] and have been used in our work. $N_{cf}(N_{c\tilde{f}})$ denote the color factors and $e_f(e_{\tilde{f}})$ the electric charges of the (s)fermions in units of the proton charge, while the scaling variables are defined as $\tau_i = 4m_i^2/M_{h/H}^2$. For large loop particle masses the form factors approach constant values,

$$\begin{aligned}
A_f^{h/H}(\tau) &\rightarrow \frac{4}{3} && \text{for } M_{h/H}^2 \ll 4m_f^2 \\
A_{\tilde{f}}^{h/H}(\tau) &\rightarrow \frac{1}{3} && \text{for } M_{h/H}^2 \ll 4m_{\tilde{f}}^2 \\
A_W^{h/H}(\tau) &\rightarrow -7 && \text{for } M_{h/H}^2 \ll 4M_W^2.
\end{aligned}$$

The reverse processes, $\gamma\gamma \rightarrow h/H$, play an important role for the MSSM Higgs search at a photon collider at high energies [21,28]. Such a photon collider can be realized by Compton back-scattering of laser light from high-energy electron beams in a linear e^+e^- collider [20]. In this collider $\gamma\gamma$ c.m. energies up to about 80% of the corresponding e^+e^- c.m. energy can be reached. The s -channel Higgs boson production cross sections are then

given by

$$\langle\sigma(\gamma\gamma \rightarrow h/H)\rangle = \frac{8\pi^2}{M_{h/H}^3}\Gamma(h/H \rightarrow \gamma\gamma)\frac{d\mathcal{L}^{\gamma\gamma}}{d\tau_{h/H}}, \quad (10)$$

where $d\mathcal{L}^{\gamma\gamma}/d\tau_{h/H}$ denotes the differential $\gamma\gamma$ luminosity for $\tau_{h/H} = M_{h/H}^2/s_{\gamma\gamma}$ with $s_{\gamma\gamma}$ being the squared c.m. energy of the photon collider. This relation between the photon fusion cross section and the photonic Higgs decay width holds in NLO QCD, too, since single gluon radiation vanishes due to the conservation of color charges as well as due to the Furry theorem.

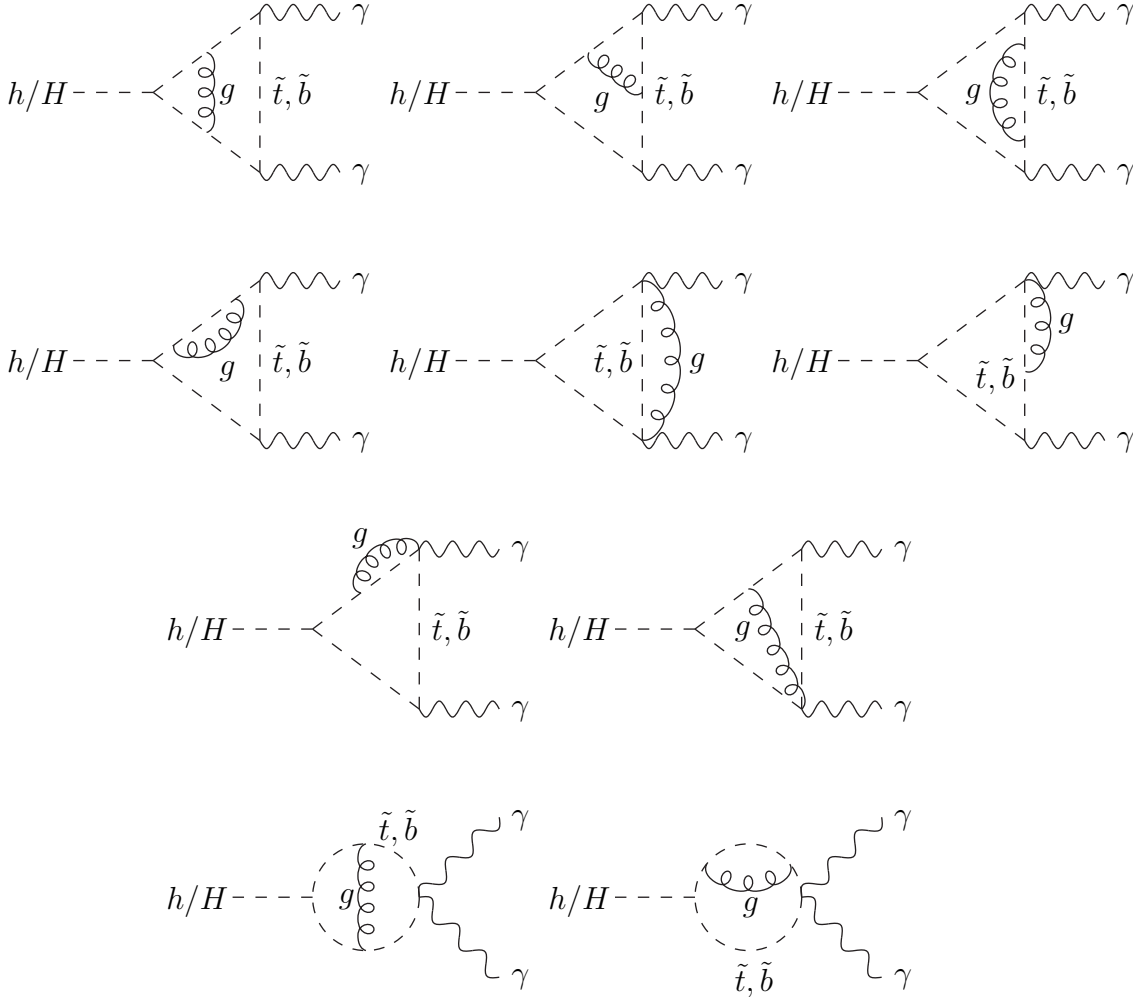


Figure 3: *Generic diagrams for the NLO QCD corrections to the squark contributions to the photonic Higgs couplings.*

The NLO QCD corrections to the photonic Higgs decay modes and the photon fusion cross section require the calculation of the two-loop diagrams depicted in Fig. 3. We have reduced the 5-dimensional Feynman parameter integrals to one-dimensional ones which

have been integrated numerically⁴. In a second calculation the QCD corrections have been obtained purely numerically. Both results agree within integration errors. The QCD corrections can be parametrized by shifts of the quark and squark amplitudes according to

$$\begin{aligned} A_Q^{h/H}(\tau_Q) &\rightarrow A_Q^{h/H}(\tau_Q) \left[1 + C_Q^{h/H}(\tau_Q) \frac{\alpha_s}{\pi} \right] \\ A_{\tilde{Q}}^{h/H}(\tau_{\tilde{Q}}) &\rightarrow A_{\tilde{Q}}^{h/H}(\tau_{\tilde{Q}}) \left[1 + C_{\tilde{Q}}^{h/H}(\tau_{\tilde{Q}}) \frac{\alpha_s}{\pi} \right]. \end{aligned} \quad (11)$$

The QCD corrections to the quark loops can be found in Refs. [22]. The corresponding coefficient $C_{\tilde{Q}}^{h/H}(\tau_{\tilde{Q}})$ of the QCD corrections to the squark loops for finite Higgs and squark masses is presented in Fig. 4 as a function of $\tau_{\tilde{Q}}$. In order to improve the perturbative behavior of the squark loop contributions they should be expressed preferably in terms of the running squark masses $m_{\tilde{Q}}(M_{\mathcal{H}}/2)$, which are related to the pole masses $M_{\tilde{Q}}$ via

$$m_{\tilde{Q}}(\mu) = M_{\tilde{Q}} \left(\frac{\alpha_s(\mu)}{\alpha_s(M_{\tilde{Q}})} \right)^{\frac{6}{\beta_0}} \quad (12)$$

where $\beta_0 = 33 - 2N_F$ with $N_F = 5$ light flavors. Their scale is identified with $\mu = M_{\mathcal{H}}/2$ within the photonic decay mode. These definitions imply a proper definition of the $\tilde{Q}\tilde{Q}$ thresholds $M_{\mathcal{H}} = 2M_{\tilde{Q}}$, without artificial displacements due to finite shifts between the *pole* and running squark masses, as is the case for the running $\overline{\text{MS}}$ masses. We have taken into account the LO scale dependence of the squark masses generated by light particle contributions.

The coefficient $C_{\tilde{Q}}^{h/H}(\tau_{\tilde{Q}})$ is real below the $\tilde{Q}\tilde{Q}$ threshold and complex above. For $\tau_{\tilde{Q}} = 1$ it diverges, so that within a margin of a few GeV around the threshold the perturbative analysis cannot be applied. This singular behavior originates from a Coulomb singularity at the threshold, since $\tilde{Q}\tilde{Q}$ pairs can form 0^{++} states. This implies that the imaginary part $\Im m C_{\tilde{Q}}^{h/H}$ develops a step due to Coulombic gluon exchange, thus resulting in a singular behavior of the real part at threshold. The singular behavior can be quantified. The lowest order form factor of the squark loops is given by

$$A_{\tilde{Q}}^{h/H,LO}(\tau) = -\tau[1 - \tau f(\tau)] \rightarrow \frac{\pi^2}{4} - 1 + i\pi\beta \quad \text{for } \tau \rightarrow 1 \quad (13)$$

where $\beta = \sqrt{1 - \tau}$ denotes the squark velocity above threshold. The QCD corrections to the imaginary part at threshold can be derived from the Sommerfeld rescattering correction [30],

$$C_{Coul} = \frac{Z}{1 - e^{-Z}} = 1 + \frac{Z}{2} + \mathcal{O}(\alpha_s^2) \quad \text{for } Z = \frac{4\pi\alpha_s}{3\beta}. \quad (14)$$

⁴Analytical results can be derived, too, as in the case of the quark loops [29].

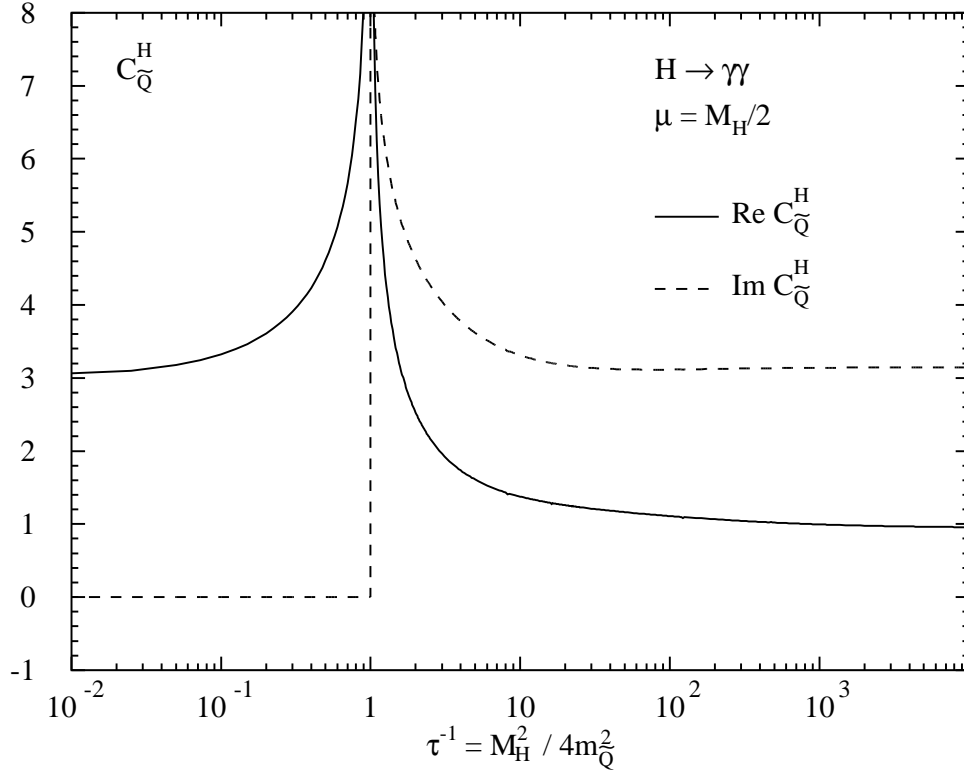


Figure 4: *Real and imaginary parts of the QCD correction factor to the squark amplitudes of the two-photon couplings for the scalar MSSM Higgs bosons. The renormalization scale of the running squark mass is taken to be $\mu = M_H/2$.*

The QCD corrected imaginary part of the $h/H\gamma\gamma$ couplings at threshold is now given as

$$\Im m A_{\tilde{Q}}^{h/H} = \pi\beta C_{coul} = \pi\beta + \frac{2\pi^2}{3}\alpha_s, \quad (15)$$

so that the real part can be derived from a once-subtracted dispersion relation yielding the following expression in the threshold region

$$A_{\tilde{Q}}^{h/H} \rightarrow A_{\tilde{Q}}^{h/H,LO} + \frac{2\pi\alpha_s}{3} \left[-\log(\tau_{\tilde{Q}}^{-1} - 1) + i\pi + const \right], \quad (16)$$

where the smooth non-singular constant is not relevant for the divergent behavior. Finally the singular behavior of the QCD correction factor at threshold can be cast into the form

$$\begin{aligned} \Re e C_{\tilde{Q}}^{h/H} &\rightarrow -\frac{8\pi^2}{3(\pi^2 - 4)} \log(\tau_{\tilde{Q}}^{-1} - 1) + const \\ \Im m C_{\tilde{Q}}^{h/H} &\rightarrow \frac{8\pi^3}{3(\pi^2 - 4)} \approx 14.09. \end{aligned} \quad (17)$$

The total size of the imaginary part and the singular behavior of the real part agree with the numerical results depicted in Fig. 4. However, the singular behaviour at threshold is

unphysical. A proper inclusion of the finite decay widths of the virtual squarks as well as a resummation of the Coulomb singularities [31] will regularize the divergences and improve the perturbative results at threshold.

In the limit of heavy squark masses the coefficient $C_{\tilde{Q}}^{h/H}(\tau_{\tilde{Q}})$ approaches a finite and constant value⁵

$$C_{\tilde{Q}}^{h/H}(\tau_{\tilde{Q}}) \rightarrow 3. \quad (18)$$

This asymptotic value can also be derived from low-energy theorems [7,8,13,32], which are based on the relation between the matrix elements with and without a light external Higgs boson. This allows the derivation of an effective Lagrangian for the Higgs couplings to photons mediated by squark loops in the heavy squark mass limit⁶

$$\Delta\mathcal{L}_{eff} = \frac{e_{\tilde{Q}}^2}{4} \frac{\beta_{\tilde{Q}}(\alpha)/\alpha}{1 + \gamma_{m_{\tilde{Q}}}(\alpha_s)} F^{\mu\nu} F_{\mu\nu} \frac{H}{v}, \quad (19)$$

where $\beta_{\tilde{Q}}(\alpha)/\alpha = (\alpha/2\pi)[1 + 4\alpha_s/\pi + \dots]$ denotes the heavy squark \tilde{Q} contribution to the QED β function and $\gamma_{m_{\tilde{Q}}}(\alpha_s) = \alpha_s/\pi + \dots$ the anomalous squark mass dimension. The NLO expansion of the effective Lagrangian reads as

$$\Delta\mathcal{L}_{eff} = e_{\tilde{Q}}^2 \frac{\alpha}{8\pi} F^{\mu\nu} F_{\mu\nu} \frac{H}{v} \left[1 + 3\frac{\alpha_s}{\pi} + \mathcal{O}(\alpha_s^2) \right], \quad (20)$$

which agrees with the $C_{\tilde{Q}}^{h/H}$ -value of Eq. (18) in the heavy squark limit.

The numerical results are presented in Figs. 5–7 for the gluophobic Higgs scenario⁷. Fig. 5 shows the partial photonic widths at NLO of the scalar Higgs bosons h, H for two values of $\text{tg}\beta = 3, 30$. The dotted lines exhibit the photonic widths without the contributions of SUSY particles, the dashed lines include all SUSY particle contributions except those of the squarks, while the full curves correspond to the full partial decay widths. For small as well as for large values of $\text{tg}\beta$ the photonic widths range between about 0.1 and 10 keV. The importance of the SUSY particles and in particular the squark contributions is clearly visible from the comparison of the three different curves. The kinks, bumps and spikes correspond to the $WW, \tilde{t}_1\tilde{t}_1, t\bar{t}, \tilde{b}_1\tilde{b}_1, \tilde{\tau}_1\tilde{\tau}_1, \tilde{\tau}_2\tilde{\tau}_2$ and $\tilde{b}_2\tilde{b}_2$ thresholds in consecutive order⁸. Due to the Coulomb singularities the stop and sbottom thresholds develop spikes corresponding to the logarithmic singularities according to Eq. (17).

The relative QCD corrections to the photonic Higgs decay widths are presented in Fig. 6 for the two cases, in which SUSY particles have been taken into account or not. The QCD corrections reach a size of 10–20% for moderate and large Higgs masses apart from

⁵This value differs from the heavy squark limit obtained in Ref. [25]. The difference can be traced back to a wrong expression for the anomalous squark mass dimension used in [25].

⁶The anomalous dimension of the kinetic photon operator $F^{\mu\nu} F_{\mu\nu}$ does not contribute at NLO [9,17].

⁷The massive QCD corrections to the quark and squark loops have been implemented in the program HDECAY [16].

⁸In the gluophobic scenario the $\tilde{\tau}$ masses amount to $m_{\tilde{\tau}_1} = 348$ GeV, $m_{\tilde{\tau}_2} = 356$ GeV for $\text{tg}\beta = 3$ and $m_{\tilde{\tau}_1} = 327$ GeV, $m_{\tilde{\tau}_2} = 377$ GeV for $\text{tg}\beta = 30$.

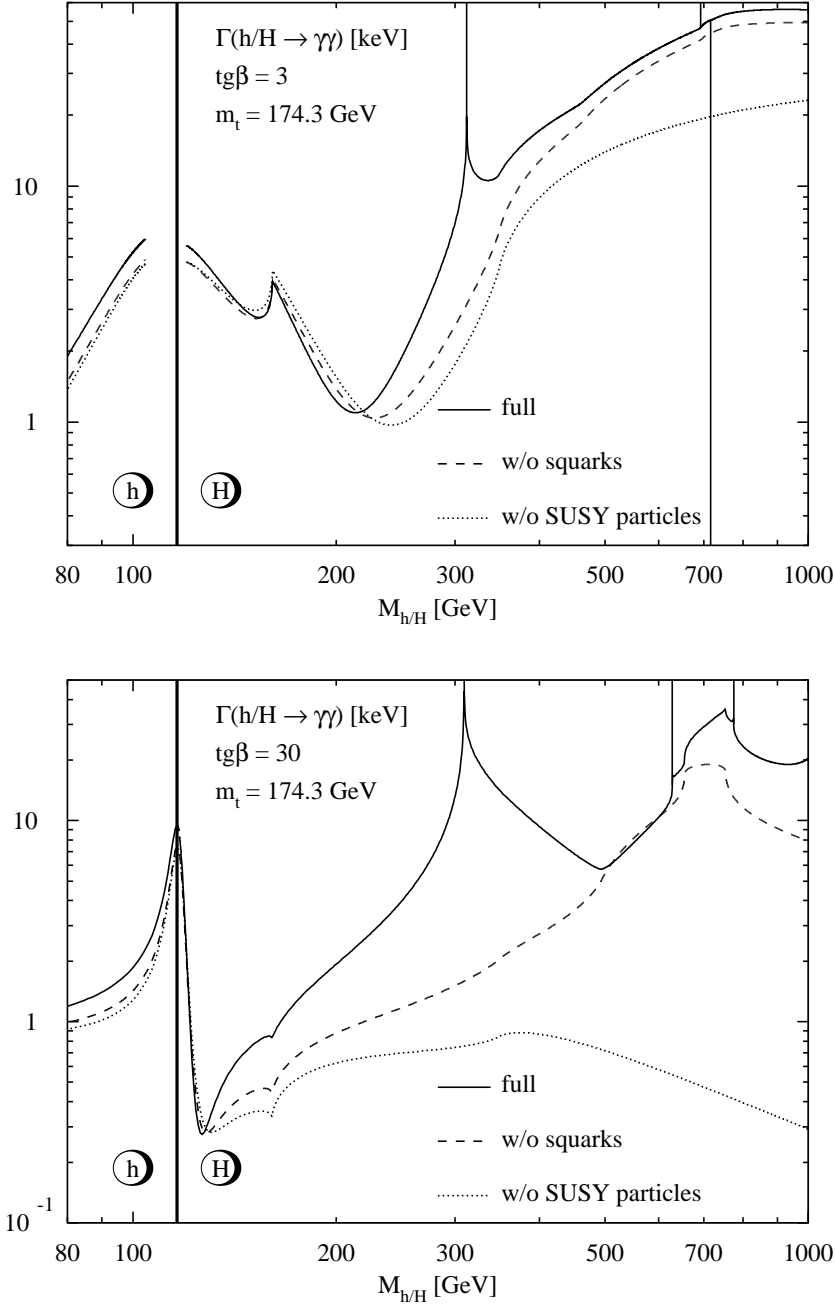


Figure 5: *QCD corrected partial decay widths of the scalar MSSM Higgs bosons to two photons as functions of the corresponding Higgs masses for $\text{tg}\beta = 3$ and 30 . The full curves include all loop contributions, in the dashed lines the squark contributions are omitted and in the dotted lines all SUSY particle loops are neglected. The kinks, bumps and spikes correspond to the WW , $\tilde{t}_1\tilde{t}_1$, $t\bar{t}$, $\tilde{b}_1\tilde{b}_1$, $\tilde{\tau}_1\tilde{\tau}_1$, $\tilde{\tau}_2\tilde{\tau}_2$ and $\tilde{b}_2\tilde{b}_2$ thresholds in consecutive order with rising Higgs mass. The renormalization scale of the running quark and squark masses is chosen to be $M_{h/H}/2$, while the scale of α_s is taken to be the corresponding Higgs mass.*

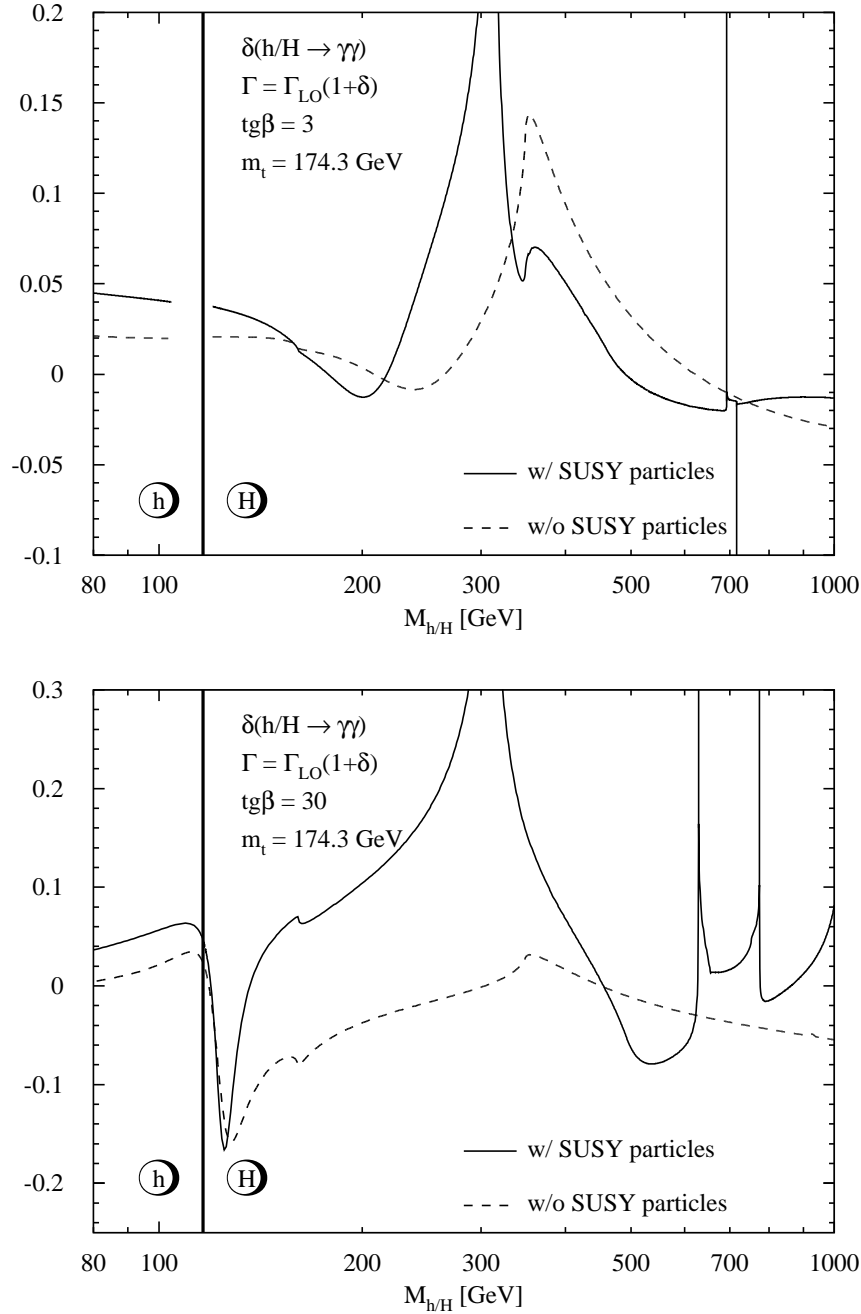


Figure 6: *Relative QCD corrections to the partial decay widths of the scalar MSSM Higgs bosons to two photons as functions of the corresponding Higgs masses for $\text{tg}\beta = 3$ and 30 . The full curves include all loop contributions while in the dashed lines the squark contributions are omitted. The kinks and spikes correspond to the WW , $\tilde{t}_1\tilde{t}_1$, $t\bar{t}$, $\tilde{b}_1\tilde{b}_1$, $\tilde{\tau}_1\tilde{\tau}_1$, $\tilde{\tau}_2\tilde{\tau}_2$ and $\tilde{b}_2\tilde{b}_2$ thresholds in consecutive order with rising Higgs mass. The renormalization scale of the running quark and squark masses is chosen to be $M_{h/H}/2$, while the scale of α_s is taken to be the corresponding Higgs mass.*

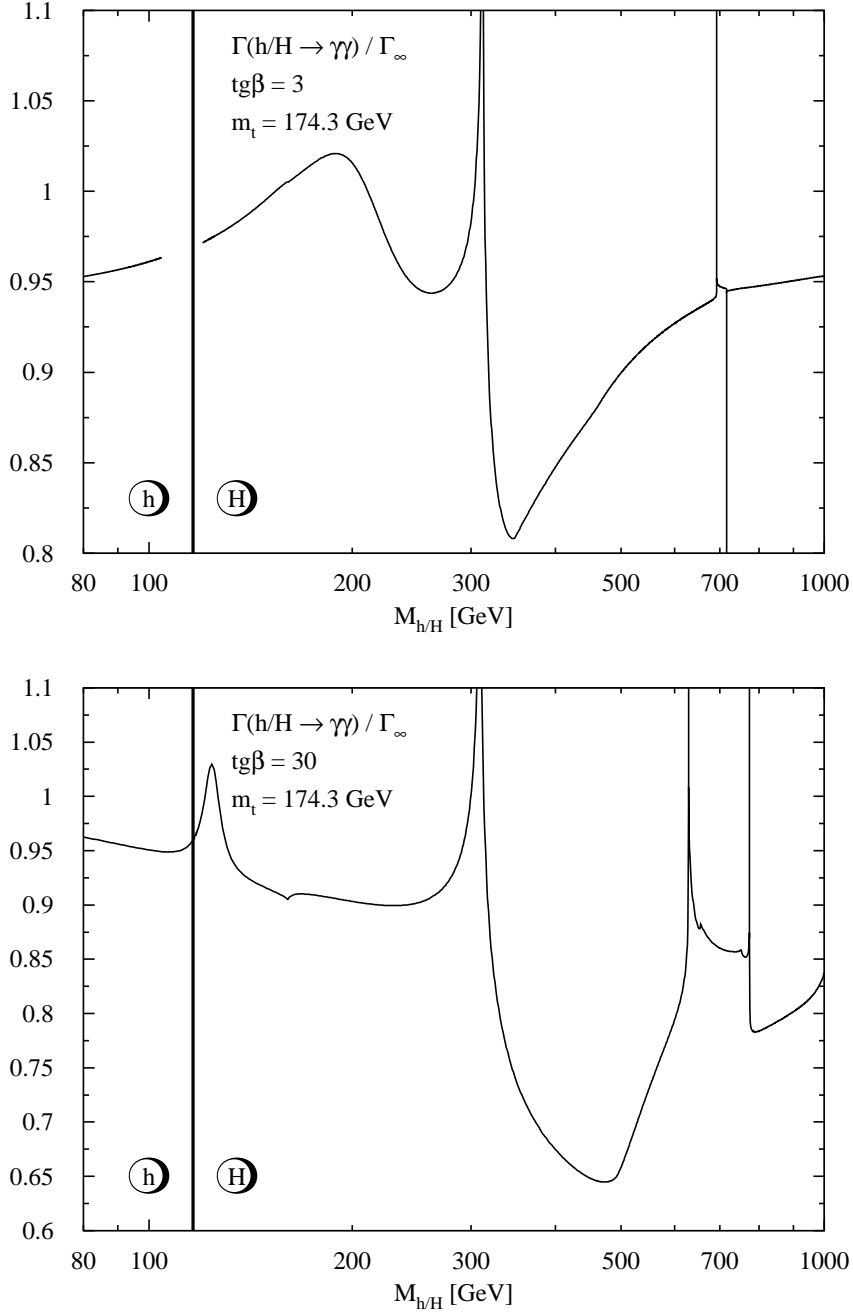


Figure 7: Ratio of the QCD corrected partial decay widths of the scalar MSSM Higgs bosons to two photons including the full squark mass dependence and those obtained by taking the relative QCD corrections to the squark loops in the heavy mass limit as functions of the corresponding Higgs masses for $\text{tg}\beta = 3$ and 30. The kinks and spikes correspond to the WW , $\tilde{t}_1\tilde{t}_1$, $t\bar{t}$, $\tilde{b}_1\tilde{b}_1$, $\tilde{\tau}_1\tilde{\tau}_1$, $\tilde{\tau}_2\tilde{\tau}_2$ and $\tilde{b}_2\tilde{b}_2$ thresholds in consecutive order with rising Higgs mass. The renormalization scale of the running quark and squark masses is chosen to be $M_{h/H}/2$, while the scale of α_s is taken to be the corresponding Higgs mass.

the threshold regions, where the perturbative results are unreliable due to the Coulomb singularities. Since at a $\gamma\gamma$ collider the photon fusion cross section can be measured with an accuracy of a few per cent, these corrections have to be taken into account properly. The size of the QCD corrections with and without SUSY particle loops is of the same order of magnitude, but they can be of opposite sign.

In order to quantify the size of squark mass effects beyond the heavy squark mass limit in the relative QCD corrections, the ratio between the fully massive photonic decay width $\Gamma(h/H \rightarrow \gamma\gamma)$ at NLO of Eqs. (9, 11) and the approximate width Γ_∞ , where the heavy squark limit of Eq. (18) has been inserted for the coefficient $C_{\tilde{Q}}^{h/H}$ instead of the fully massive result, is shown in Fig. 7. (The full squark mass dependence of the LO form factors has been taken into account in both expressions.) The squark mass effects reach a size of up to $\sim 30\%$, thus underlining the relevance of including the full mass dependences.

2.2 Gluonic Scalar Higgs Decays

The gluonic Higgs boson decays $h/H \rightarrow gg$ are mediated by quark and squark triangle loops (see Fig. 1). The lowest order decay widths of the scalar MSSM Higgs boson decays are given by [7,8]

$$\Gamma_{LO}(h/H \rightarrow gg) = \frac{G_F \alpha_s^2(\mu_R) M_{h/H}^3}{36\sqrt{2}\pi^3} \left| \sum_Q g_Q^{h/H} A_Q^{h/H}(\tau_Q) + \sum_{\tilde{Q}} g_{\tilde{Q}}^{h/H} A_{\tilde{Q}}^{h/H}(\tau_{\tilde{Q}}) \right|^2 \quad (21)$$

$$A_Q^{h/H}(\tau) = \frac{3}{2}\tau[1 + (1 - \tau)f(\tau)]$$

$$A_{\tilde{Q}}^{h/H}(\tau) = -\frac{3}{4}\tau[1 - \tau f(\tau)]$$

using the same notation as for the photonic Higgs boson decays. For large loop particle masses the form factors approach constant values,

$$A_Q^{h/H}(\tau) \rightarrow 1 \quad \text{for } M_{h/H}^2 \ll 4m_Q^2$$

$$A_{\tilde{Q}}^{h/H}(\tau) \rightarrow \frac{1}{4} \quad \text{for } M_{h/H}^2 \ll 4m_{\tilde{Q}}^2.$$

The squark contributions become significant for squark masses below about 400 GeV.

The NLO QCD corrections to the gluonic decay widths are known to be large [8,17, 18,19]. They can be decomposed into the two-loop virtual corrections and the one-loop real corrections determined by the real radiation processes

$$h/H \rightarrow ggg \quad \text{and} \quad gq\bar{q}.$$

The generic Feynman diagrams for the squark loop contributions are depicted in Figs. 8 and 9. As in the photonic case the Feynman integrals of the virtual corrections have been reduced to one-dimensional integrals, which have been evaluated numerically. In a second

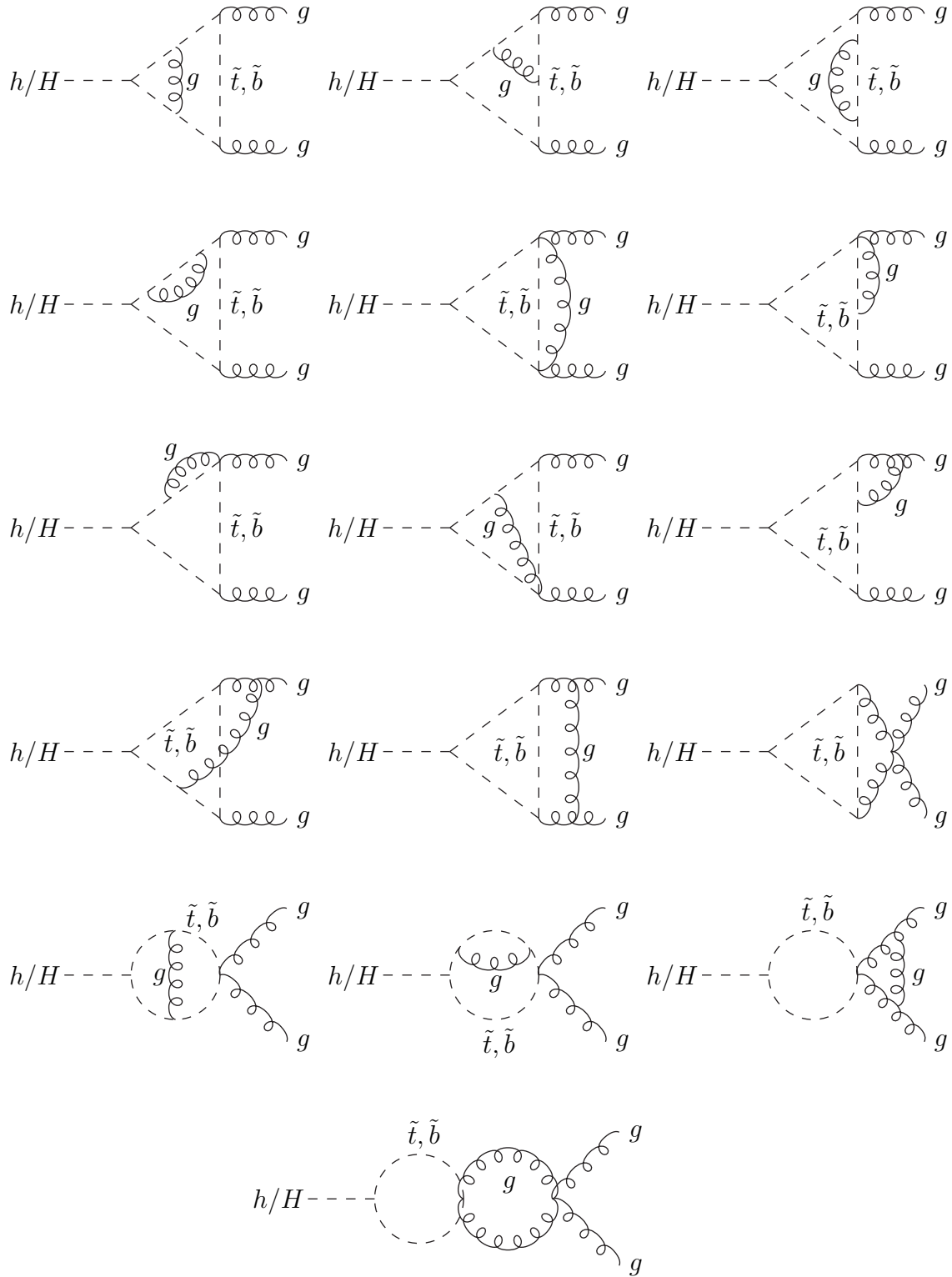


Figure 8: *Generic diagrams for the virtual NLO QCD corrections to the squark contributions to the gluonic Higgs couplings.*

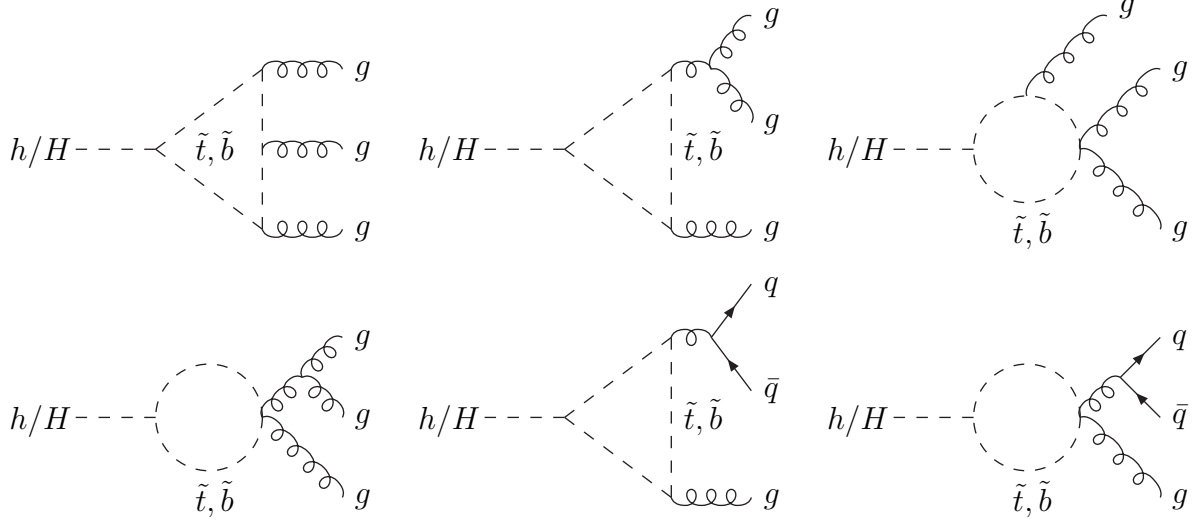


Figure 9: *Typical diagrams for the real NLO QCD corrections to the squark contributions to the gluonic Higgs decays.*

calculation the results have been obtained purely numerically. Both results are in mutual agreement.

The strong coupling constant α_s is renormalized in the $\overline{\text{MS}}$ scheme, with the top quark and squark contributions decoupled from the scale dependence, and the quark and squark masses are renormalized on-shell. The result can be cast into the form

$$\begin{aligned}
\Gamma(h/H \rightarrow gg) &= \Gamma_{LO}(h/H \rightarrow gg) \left\{ 1 + E^{h/H} \frac{\alpha_s}{\pi} \right\} \\
E^{h/H} &= \frac{95}{4} - \frac{7}{6} N_F + \frac{7}{2} \Re \left\{ \frac{\sum_{\tilde{Q}} g_{\tilde{Q}}^{h/H} A_{\tilde{Q}}^{h/H}(\tau_{\tilde{Q}})}{\sum_Q g_Q^{h/H} A_Q^{h/H}(\tau_Q) + \sum_{\tilde{Q}} g_{\tilde{Q}}^{h/H} A_{\tilde{Q}}^{h/H}(\tau_{\tilde{Q}})} \right\} \\
&+ \frac{33 - 2N_F}{6} \log \frac{\mu_R^2}{M_{h/H}^2} + \Delta E^{h/H},
\end{aligned} \tag{22}$$

where the correction $\Delta E^{h/H}$ denotes the Higgs, quark and squark mass dependent part, while the rest represents the total result in the limit of heavy loop particle masses. The latter can be derived from low-energy theorems analogously to the photonic case. The squark contributions to the gluonic Higgs couplings in the limit of large squark masses arise from the effective Lagrangian [$\mathcal{H} = h, H$]

$$\Delta \mathcal{L}_{eff} = g_{\tilde{Q}}^{\mathcal{H}} \frac{1}{4} \frac{\beta_{\tilde{Q}}(\alpha_s)/\alpha_s}{1 + \gamma_{m_{\tilde{Q}}}(\alpha_s)} G^{a\mu\nu} G_{\mu\nu}^a \frac{\mathcal{H}}{v}, \tag{23}$$

where $\beta_{\tilde{Q}}(\alpha_s)/\alpha_s = (\alpha_s/12\pi)[1 + 11\alpha_s/2\pi + \dots]$ denotes the heavy squark contribution to the QCD β function and $\gamma_{m_{\tilde{Q}}}(\alpha_s) = \alpha_s/\pi + \dots$ the anomalous squark mass dimension.

The NLO expansion of the effective Lagrangian reads as⁹

$$\Delta\mathcal{L}_{eff} = g_{\tilde{Q}}^{\mathcal{H}} \frac{\alpha_s}{48\pi} G^{a\mu\nu} G_{\mu\nu}^a \frac{\mathcal{H}}{v} \left[1 + \frac{9}{2} \frac{\alpha_s}{\pi} + \mathcal{O}(\alpha_s^2) \right]. \quad (24)$$

Including the quark contributions in the heavy quark limit, the total effective Lagrangian is given by

$$\mathcal{L}_{eff} = \frac{\alpha_s}{12\pi} G^{a\mu\nu} G_{\mu\nu}^a \frac{\mathcal{H}}{v} \left\{ \sum_Q g_Q^{\mathcal{H}} \left[1 + \frac{11}{4} \frac{\alpha_s}{\pi} \right] + \sum_{\tilde{Q}} \frac{g_{\tilde{Q}}^{\mathcal{H}}}{4} \left[1 + \frac{9}{2} \frac{\alpha_s}{\pi} \right] + \mathcal{O}(\alpha_s^2) \right\}, \quad (25)$$

The calculation based on this effective Lagrangian yields the following results for the finite parts of the individual contributions to the coefficients $E^{h/H}$,

$$\begin{aligned} E^{h/H} &= E_{virt}^{h/H} + E_{ggg}^{h/H} + E_{gq\bar{q}}^{h/H} + \frac{33 - 2N_F}{6} \log \frac{\mu_R^2}{M_{h/H}^2} \\ E_{virt}^{h/H} &= \pi^2 + \frac{11}{2} + \frac{7}{2} \Re e \left\{ \frac{\sum_{\tilde{Q}} g_{\tilde{Q}}^{h/H} A_{\tilde{Q}}^{h/H}(\tau_{\tilde{Q}})}{\sum_Q g_Q^{h/H} A_Q^{h/H}(\tau_Q) + \sum_{\tilde{Q}} g_{\tilde{Q}}^{h/H} A_{\tilde{Q}}^{h/H}(\tau_{\tilde{Q}})} \right\} \\ E_{ggg}^{h/H} &= -\pi^2 + \frac{73}{4} \\ E_{gq\bar{q}}^{h/H} &= -\frac{7}{6} N_F, \end{aligned} \quad (26)$$

which agrees with the explicit results for the coefficients $E^{h/H}$ of Eq. (22) in the heavy quark and squark limits, where $\Delta E^{h/H}$ vanishes.

Since at the $\tilde{Q}\tilde{Q}$ thresholds 0^{++} states can form, the NLO QCD corrections exhibit Coulomb singularities as for the photonic Higgs couplings. The singular behavior can be derived from the Sommerfeld rescattering corrections and leads to the following expressions at each specific $\tilde{Q}_0\tilde{Q}_0$ threshold,

$$E^{h/H} \rightarrow \Re e \left\{ \frac{g_{\tilde{Q}_0}^{h/H} A_{\tilde{Q}_0}^{h/H}(\tau_{\tilde{Q}_0}) \frac{16\pi^2}{3(\pi^2-4)} \left[-\log(\tau_{\tilde{Q}_0}^{-1} - 1) + i\pi + const \right]}{\sum_Q g_Q^{h/H} A_Q^{h/H}(\tau_Q) + \sum_{\tilde{Q}} g_{\tilde{Q}}^{h/H} A_{\tilde{Q}}^{h/H}(\tau_{\tilde{Q}})} \right\}, \quad (27)$$

which agrees quantitatively with the numerical results.

The partial decay widths into gluons are presented in Fig. 10 with and without the squark contributions for two values of $\text{tg}\beta = 3, 30$ in the gluophobic Higgs scenario. The renormalization scale has been identified with the corresponding Higgs mass, $\mu_R = M_{h/H}$. The partial widths range between 10^{-2} and 10 MeV. The comparison of the two curves underlines the large size of the squark contributions, which are of the same order as the

⁹The value for the QCD corrections in the heavy squark limit differs from the result obtained in Ref. [13]. The difference can be traced back to a wrong expression for the anomalous squark mass dimension used in [13].

quark loops in this scenario. The spikes of the full results originate from the Coulomb singularities of the $\tilde{t}_1\tilde{t}_1$, $\tilde{b}_1\tilde{b}_1$ and $\tilde{b}_2\tilde{b}_2$ thresholds in consecutive order.

Fig. 11 displays the relative QCD corrections to the gluonic Higgs decays with and without squark contributions. Apart from the threshold singularities they are of similar size and increase the decay widths by $\mathcal{O}(50\%)$.

In order to quantify the squark mass effects on the relative QCD corrections, Fig. 12 depicts the ratio between the fully massive gluonic decay widths $\Gamma(h/H \rightarrow gg)$ and the widths obtained by taking the squark contributions to the coefficients $E^{h/H}$ in the infinite squark mass limits, while the LO decay widths are used with the full squark mass dependence. It is clearly visible that squark mass effects on the relative NLO corrections can reach 20–30% in addition to the squark mass dependence at LO. Thus the fully massive results are significant for a proper quantitative prediction of the gluonic decay widths at NLO. The heavy squark mass limit turns out to be less reliable than the heavy top mass limit for the top quark loops.

2.3 Gluon Fusion

The gluon fusion processes $gg \rightarrow h/H$ are mediated by heavy quark and squark triangle loops with the latter contributing significantly for squark masses below 400 GeV. The lowest order cross sections in the narrow-width approximation can be obtained from the gluonic decay widths of the scalar Higgs bosons [7,8,33],

$$\begin{aligned} \sigma_{LO}(pp \rightarrow h/H) &= \sigma_0^{h/H} \tau_{h/H} \frac{d\mathcal{L}^{gg}}{d\tau_{h/H}} & (28) \\ \sigma_0^{h/H} &= \frac{\pi^2}{8M_{h/H}^3} \Gamma_{LO}(h/H \rightarrow gg) \\ \sigma_0^{h/H} &= \frac{G_F \alpha_s^2(\mu_R)}{288\sqrt{2}\pi} \left| \sum_Q g_Q^{h/H} A_Q^{h/H}(\tau_Q) + \sum_{\tilde{Q}} g_{\tilde{Q}}^{h/H} A_{\tilde{Q}}^{h/H}(\tau_{\tilde{Q}}) \right|^2, & (29) \end{aligned}$$

where $\tau_{h/H} = M_{h/H}^2/s$ with s specifying the squared hadronic c.m. energy. The LO form factors are identical to the corresponding form factors $A_{Q/\tilde{Q}}^{h/H}$ of the gluonic decay modes, Eq. (21). The gluon luminosity at the factorization scale μ_F is defined as

$$\frac{d\mathcal{L}^{gg}}{d\tau} = \int_\tau^1 \frac{dx}{x} g(x, \mu_F^2) g(\tau/x, \mu_F^2),$$

where $g(x, \mu_F^2)$ denotes the gluon parton density of the proton.

The NLO QCD corrections consist of the virtual two-loop corrections, corresponding to the diagrams of Fig. 8, as well as the real corrections due to the radiation processes $gg \rightarrow gh/H$, $gq \rightarrow qh/H$ and $q\bar{q} \rightarrow gh/H$. The diagrams of the real corrections are shown in Fig. 13. While the Higgs bosons do not acquire any transverse momentum at LO, they appear at finite transverse momenta in these radiation processes corresponding to Higgs

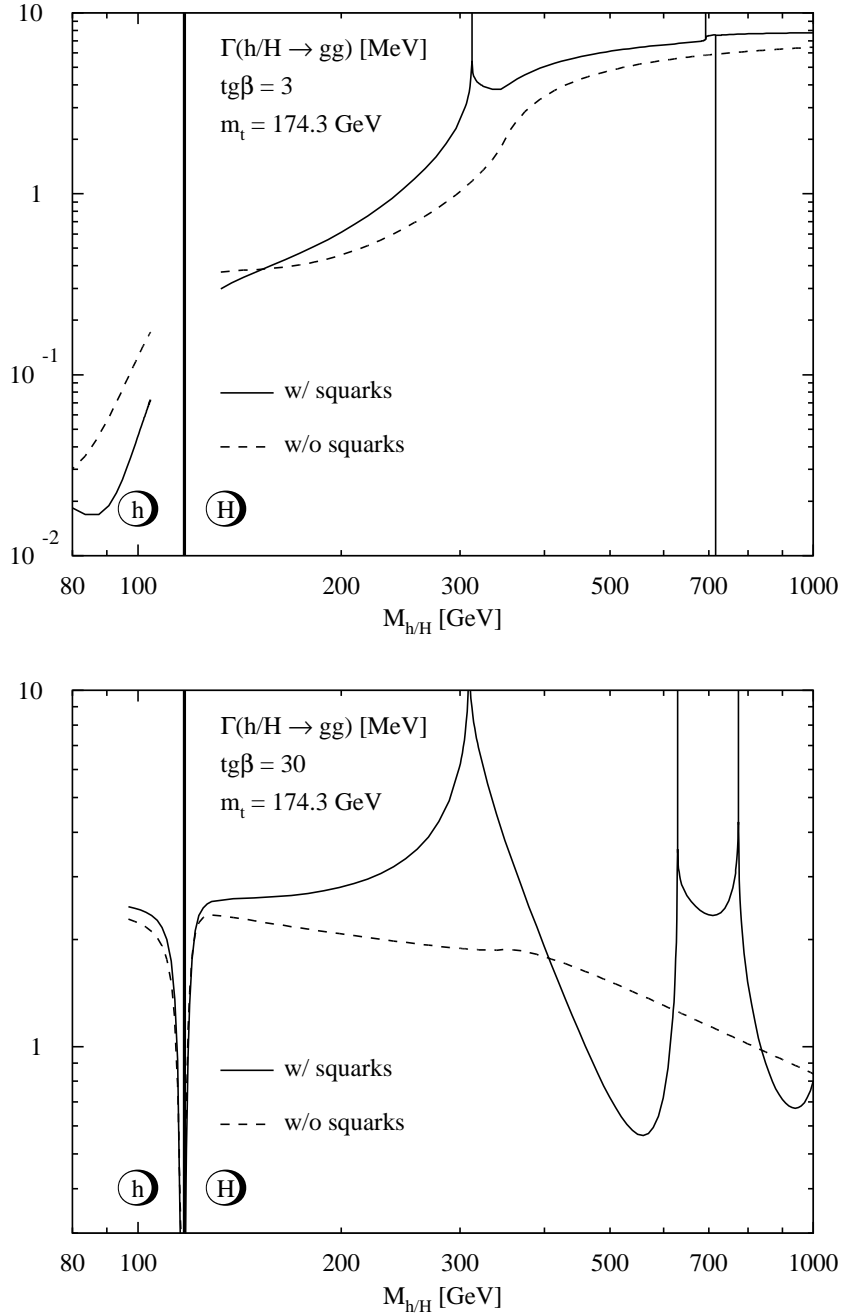


Figure 10: *QCD corrected partial decay widths of the scalar MSSM Higgs bosons to two gluons as functions of the corresponding Higgs masses for $\tan\beta = 3$ and 30 . The full curves include all loop contributions, while in the dashed lines the squark contributions are omitted. The kinks, bumps and spikes correspond to the $\tilde{t}_1\tilde{t}_1$, $t\bar{t}$, $\tilde{b}_1\tilde{b}_1$ and $\tilde{b}_2\tilde{b}_2$ thresholds in consecutive order with rising Higgs mass. The renormalization scale of the strong coupling α_s is chosen as the corresponding Higgs mass.*

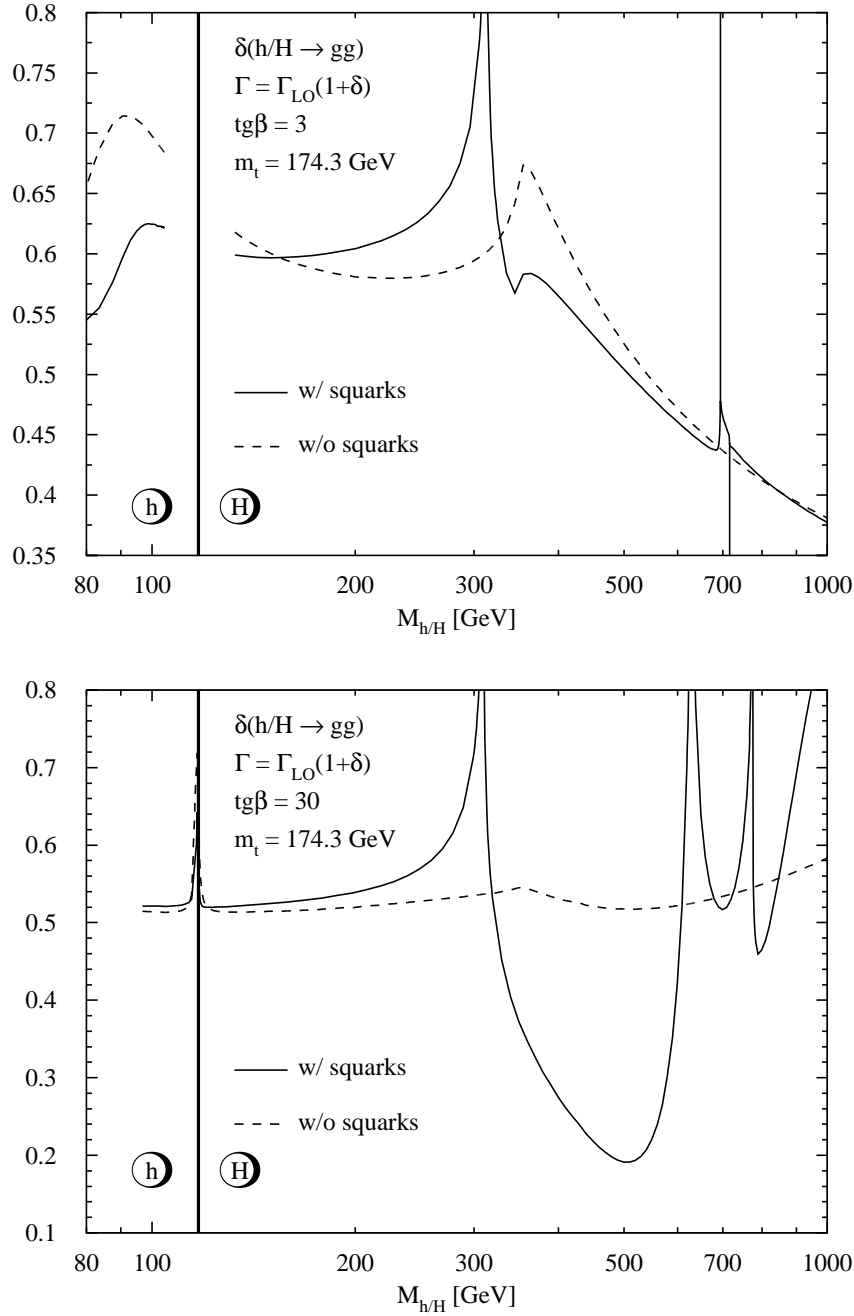


Figure 11: *Relative QCD corrections to the partial decay widths of the scalar MSSM Higgs bosons to two gluons as functions of the corresponding Higgs masses for $\text{tg}\beta = 3$ and 30. The full curves include all loop contributions, while in the dashed lines the squark contributions are omitted. The kinks, bumps and spikes correspond to the $\tilde{t}_1\tilde{t}_1$, $t\bar{t}$, $\tilde{b}_1\tilde{b}_1$ and $\tilde{b}_2\tilde{b}_2$ thresholds in consecutive order with rising Higgs mass. The renormalization scale of the strong coupling α_s is chosen as the corresponding Higgs mass.*

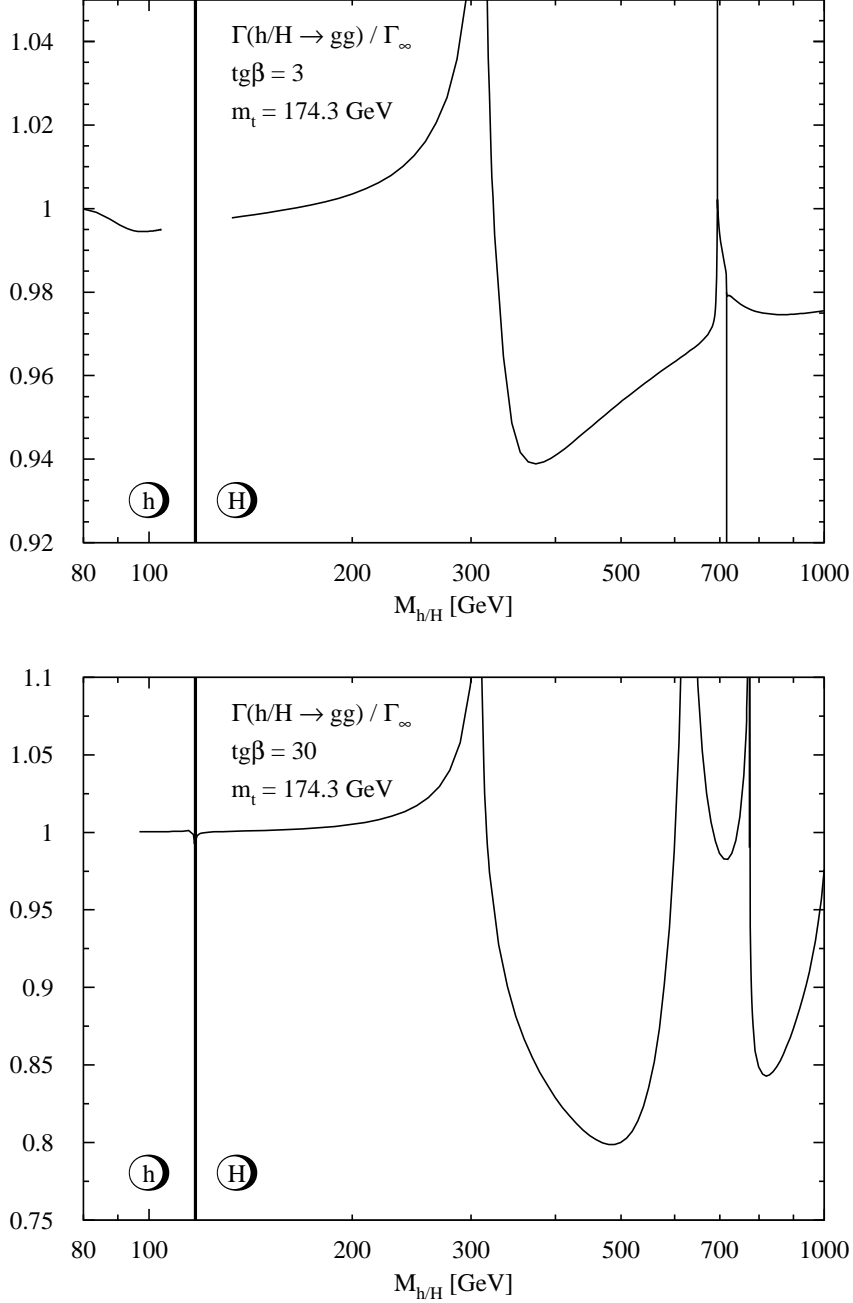


Figure 12: Ratio of the QCD corrected partial decay widths of the scalar MSSM Higgs bosons to two gluons including the full squark mass dependence and those obtained by taking the relative QCD corrections to the squark loops in the heavy mass limit as functions of the corresponding Higgs masses for $\tan\beta = 3$ and 30. The kinks and spikes correspond to the $\tilde{t}_1\tilde{t}_1$, $\tilde{b}_1\tilde{b}_1$ and $\tilde{b}_2\tilde{b}_2$ thresholds in consecutive order with rising Higgs mass. The renormalization scale of the strong coupling α_s is chosen as the corresponding Higgs mass.

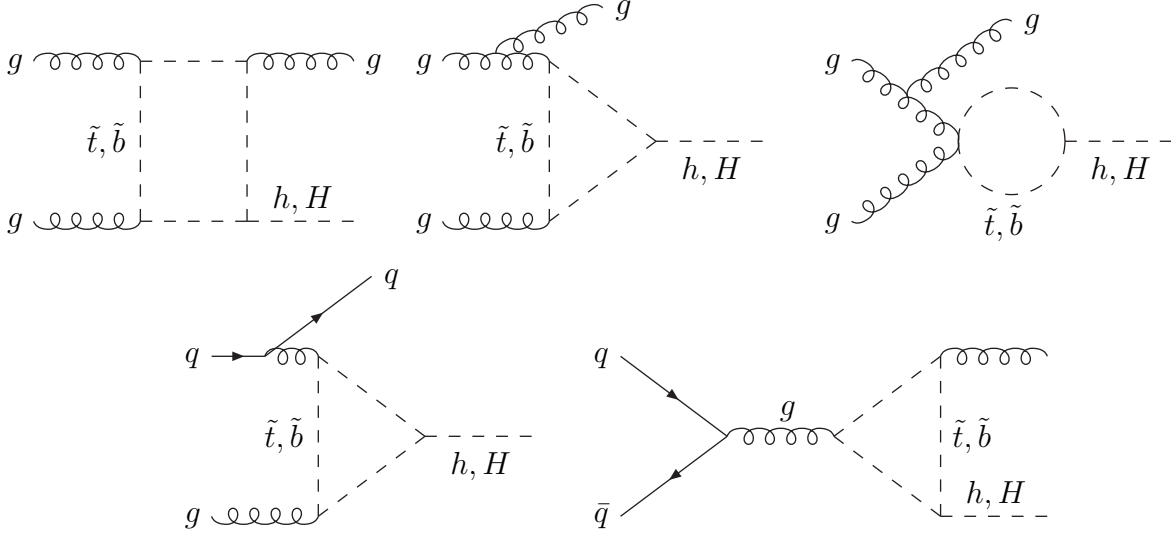


Figure 13: *Typical diagrams for the real NLO QCD corrections to the squark contributions to the gluon fusion processes.*

+ jet production. The relevance of quark mass effects on the shapes of the transverse momentum distributions has been demonstrated in Ref. [34], so that similar effects may be expected for the squark mass dependence. The final results for the total hadronic cross sections can be split into five parts accordingly,

$$\sigma(pp \rightarrow h/H + X) = \sigma_0^{h/H} \left[1 + C^{h/H} \frac{\alpha_s}{\pi} \right] \tau_{h/H} \frac{d\mathcal{L}^{gg}}{d\tau_{h/H}} + \Delta\sigma_{gg}^{h/H} + \Delta\sigma_{gq}^{h/H} + \Delta\sigma_{q\bar{q}}^{h/H}, \quad (30)$$

The strong coupling constant is renormalized in the $\overline{\text{MS}}$ scheme, with the top quark and squark contributions decoupled from the scale dependence. The quark and squark masses are renormalized on-shell. The parton densities are defined in the $\overline{\text{MS}}$ scheme with five active flavors, i.e. the top quark and the squarks are not included in the factorization scale dependence. The virtual coefficients split into the infrared π^2 term, a logarithmic term including the renormalization scale μ_R and finite (s)quark mass dependent pieces $c^{h/H}(\tau_Q, \tau_{\tilde{Q}})$,

$$C^{h/H}(\tau_Q, \tau_{\tilde{Q}}) = \pi^2 + c^{h/H}(\tau_Q, \tau_{\tilde{Q}}) + \frac{33 - 2N_F}{6} \log \frac{\mu_R^2}{M_{h/H}^2}. \quad (31)$$

The finite hard contributions from gluon radiation as well as gq and $q\bar{q}$ scattering depend after mass factorization on the renormalization and factorization scales μ_R, μ_F and are given by

$$\Delta\sigma_{gg}^{h/H} = \int_{\tau_{h/H}}^1 d\tau \frac{d\mathcal{L}^{gg}}{d\tau} \times \frac{\alpha_s}{\pi} \sigma_0^{h/H} \left\{ -z P_{gg}(z) \log \frac{\mu_F^2}{\hat{s}} + d_{gg}^{h/H}(z, \tau_Q, \tau_{\tilde{Q}}) \right\}$$

$$\begin{aligned}
& +12 \left[\left(\frac{\log(1-z)}{1-z} \right)_+ - z[2-z(1-z)] \log(1-z) \right] \Big\} \\
\Delta\sigma_{gq}^{h/H} &= \int_{\tau_H}^1 d\tau \sum_{q,\bar{q}} \frac{d\mathcal{L}^{gq}}{d\tau} \times \frac{\alpha_s}{\pi} \sigma_0^{h/H} \left\{ -\frac{z}{2} P_{gq}(z) \log \frac{\mu_F^2}{\hat{s}(1-z)^2} + d_{gq}^{h/H}(z, \tau_Q, \tau_{\bar{Q}}) \right\} \\
\Delta\sigma_{q\bar{q}}^{h/H} &= \int_{\tau_H}^1 d\tau \sum_q \frac{d\mathcal{L}^{q\bar{q}}}{d\tau} \times \frac{\alpha_s}{\pi} \sigma_0^{h/H} d_{q\bar{q}}^{h/H}(z, \tau_Q, \tau_{\bar{Q}}), \tag{32}
\end{aligned}$$

with $z = \tau_{h/H}/\tau = M_{h/H}^2/\hat{s}$, where \hat{s} denotes the squared partonic c.m. energy; P_{gg} and P_{gq} are the standard Altarelli–Parisi splitting functions [35]:

$$\begin{aligned}
P_{gg}(z) &= 6 \left\{ \left(\frac{1}{1-z} \right)_+ + \frac{1}{z} - 2 + z(1-z) \right\} + \frac{33-2N_F}{6} \delta(1-z) \\
P_{gq}(z) &= \frac{4}{3} \frac{1+(1-z)^2}{z}. \tag{33}
\end{aligned}$$

The natural scale choices turn out to be $\mu_R = \mu_F = M_{h/H}$. The quark and squark mass dependences are contained in the in the kernels $c^{h/H}(\tau_Q, \tau_{\bar{Q}})$ and $d_{ij}^{h/H}(z, \tau_Q, \tau_{\bar{Q}})$ in addition to the LO coefficients $\sigma_0^{h/H}$. In the heavy loop particle mass limit they reduce to simple expressions,

$$\begin{aligned}
c^{h/H}(\tau_Q, \tau_{\bar{Q}}) &\rightarrow \frac{11}{2} + \frac{7}{2} \Re e \left\{ \frac{\sum_{\bar{Q}} g_{\bar{Q}}^{h/H} A_{\bar{Q}}^{h/H}(\tau_{\bar{Q}})}{\sum_Q g_Q^{h/H} A_Q^{h/H}(\tau_Q) + \sum_{\bar{Q}} g_{\bar{Q}}^{h/H} A_{\bar{Q}}^{h/H}(\tau_{\bar{Q}})} \right\} \\
d_{gg}^{h/H}(z, \tau_Q, \tau_{\bar{Q}}) &\rightarrow -\frac{11}{2}(1-z)^3 \\
d_{gq}^{h/H}(z, \tau_Q, \tau_{\bar{Q}}) &\rightarrow \frac{2}{3}z^2 - (1-z)^2 \\
d_{q\bar{q}}^{h/H}(z, \tau_Q, \tau_{\bar{Q}}) &\rightarrow \frac{32}{27}(1-z)^3. \tag{34}
\end{aligned}$$

These can also be derived from the effective Lagrangian Eq. (25), so that the full calculation agrees with the derivation from the low-energy theorems in the heavy loop particle mass limits.

Due to the formation of 0^{++} states at the $\tilde{Q}\tilde{Q}$ thresholds the NLO QCD corrections develop Coulomb singularities analogous to the photonic Higgs decay modes. The singular behavior can be derived from the Sommerfeld rescattering corrections in the same way as in the photonic case, leading to the following expressions at each specific $\tilde{Q}_0\tilde{Q}_0$ threshold,

$$c^{h/H} \rightarrow \Re e \left\{ \frac{g_{\tilde{Q}_0}^{h/H} A_{\tilde{Q}_0}^{h/H}(\tau_{\tilde{Q}_0}) \frac{16\pi^2}{3(\pi^2-4)} \left[-\log(\tau_{\tilde{Q}_0}^{-1}-1) + i\pi + const \right]}{\sum_Q g_Q^{h/H} A_Q^{h/H}(\tau_Q) + \sum_{\bar{Q}} g_{\bar{Q}}^{h/H} A_{\bar{Q}}^{h/H}(\tau_{\bar{Q}})} \right\}, \tag{35}$$

which agrees quantitatively with the numerical results.

The total gluon fusion cross section at NLO is displayed in Fig. 14 with and without squark loop contributions. The renormalization and factorization scales have been identified with the corresponding Higgs mass, $\mu_R = \mu_F = M_{h/H}$. In the gluophobic Higgs scenario the squark loops alter the size of the cross sections by up to factors of about three. The spikes of the full curves originate from the Coulomb singularities at the $\tilde{t}_1\tilde{t}_1$, $\tilde{b}_1\tilde{b}_1$ and $\tilde{b}_2\tilde{b}_2$ thresholds in consecutive order analogously to the photonic and gluonic Higgs couplings. It can be inferred from Fig. 14 that squark effects are always important, if the Higgs mass exceeds the corresponding squark-antisquark threshold. This is confirmed in particular for large values of $\text{tg}\beta$, where the top quark contribution is less important, but sizeable squark effects are visible close to and beyond the different thresholds. This feature also holds in other MSSM scenarios.

The LO and NLO cross sections are shown in Fig. 15. The QCD corrections increase the gluon fusion cross sections by 10–100%, but can be significantly larger in regions of large destructive interferences between quark and squark loops, as is the case for very large Higgs masses for $\text{tg}\beta = 30$. The corrections are of very similar size for the quark and squark loops individually in agreement with the results of Ref. [13]. In spite of the large corrections the residual scale dependence is reduced from about 50% at LO to $\sim 20\%$ at NLO and indicates a significant stabilization of the theoretical predictions. This agrees with the former results for the quark loop contributions [8,10]. Based on the approximate NNLO and NNNLO results in the limit of heavy top quarks a further moderate increase by less than 20–30% can be expected beyond NLO for small and moderate values of $\text{tg}\beta$. For large values of $\text{tg}\beta$, however, the size of the NLO corrections is moderate in regions without strong destructive interference effects between the quark and squark loops and the scale dependence is small. This signalizes a much more reliable result after including the NLO corrections. The residual theoretical uncertainties of our NLO results can be estimated to less than about 20%.

The squark mass effects on the K factors are exemplified in Fig. 16, where the ratios of the NLO cross sections are displayed, including the full mass dependence, and of the NLO cross sections, where the coefficients $c^{h/H}(\tau_Q, \tau_{\tilde{Q}})$ and $d_{ij}^{h/H}(z, \tau_Q, \tau_{\tilde{Q}})$ are used in the heavy squark limits ($\tau_{\tilde{Q}} \rightarrow \infty$). In addition to the squark mass dependence of the LO cross sections, the K factors develop a squark mass dependence of up to about 20%, thus supporting the relevance of our results compared to the previous results of Ref. [13]. The squark mass effects on the K factors turn out to be larger than the corresponding quark mass effects [9]. In addition they are larger than the residual theoretical uncertainties and cannot be neglected in realistic analyses. Since the gluino contributions are expected to be much smaller, the squark mass dependence obtained in this work will be the dominant part of the differences between the heavy mass limits and a full MSSM calculation at NLO.

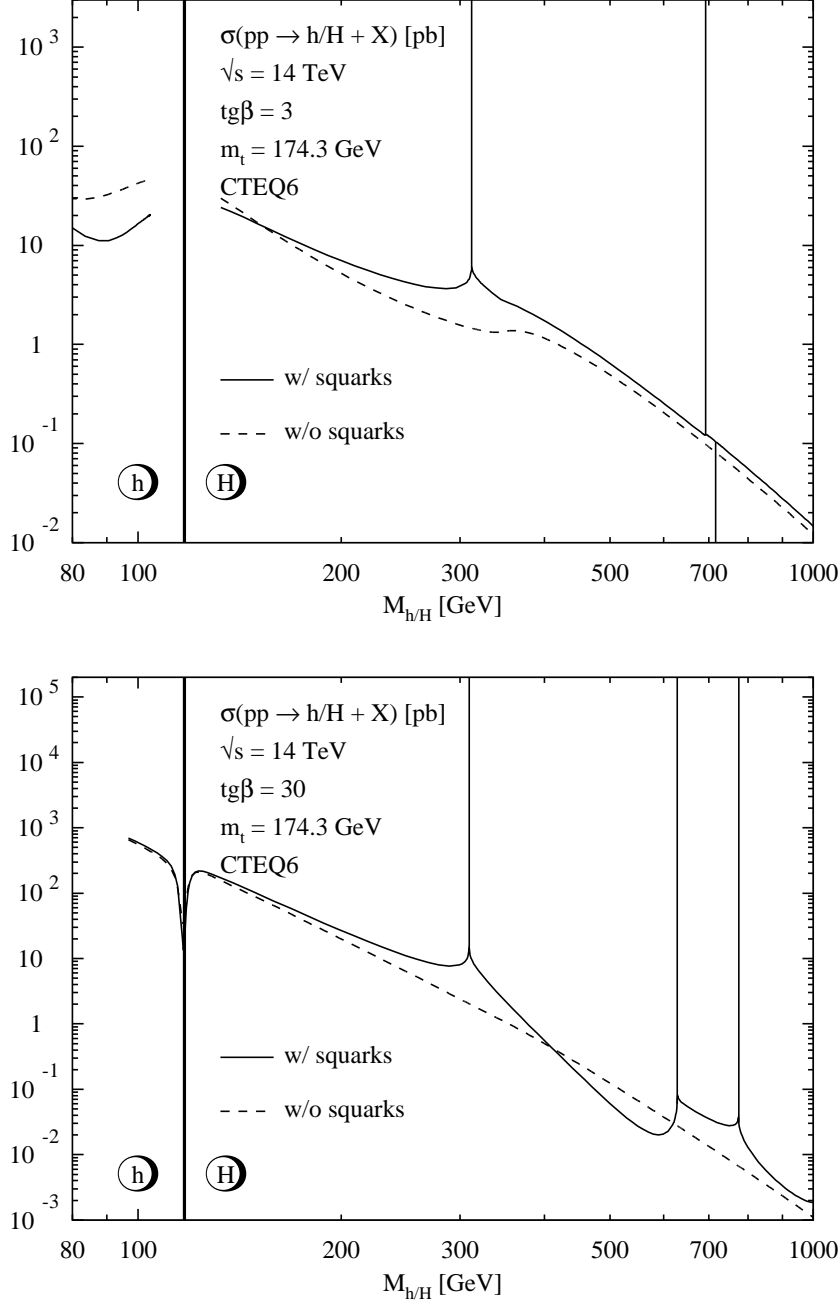


Figure 14: QCD corrected production cross sections of the scalar MSSM Higgs bosons via gluon fusion as functions of the corresponding Higgs masses for $\tan\beta = 3$ and 30. The full curves include all loop contributions, while in the dashed lines the squark contributions are omitted. The kinks, bumps and spikes correspond to the $\tilde{t}_1\tilde{t}_1$, $t\bar{t}$, $\tilde{b}_1\tilde{b}_1$ and $\tilde{b}_2\tilde{b}_2$ thresholds in consecutive order with rising Higgs mass. The renormalization and factorization scales are chosen as the corresponding Higgs mass.

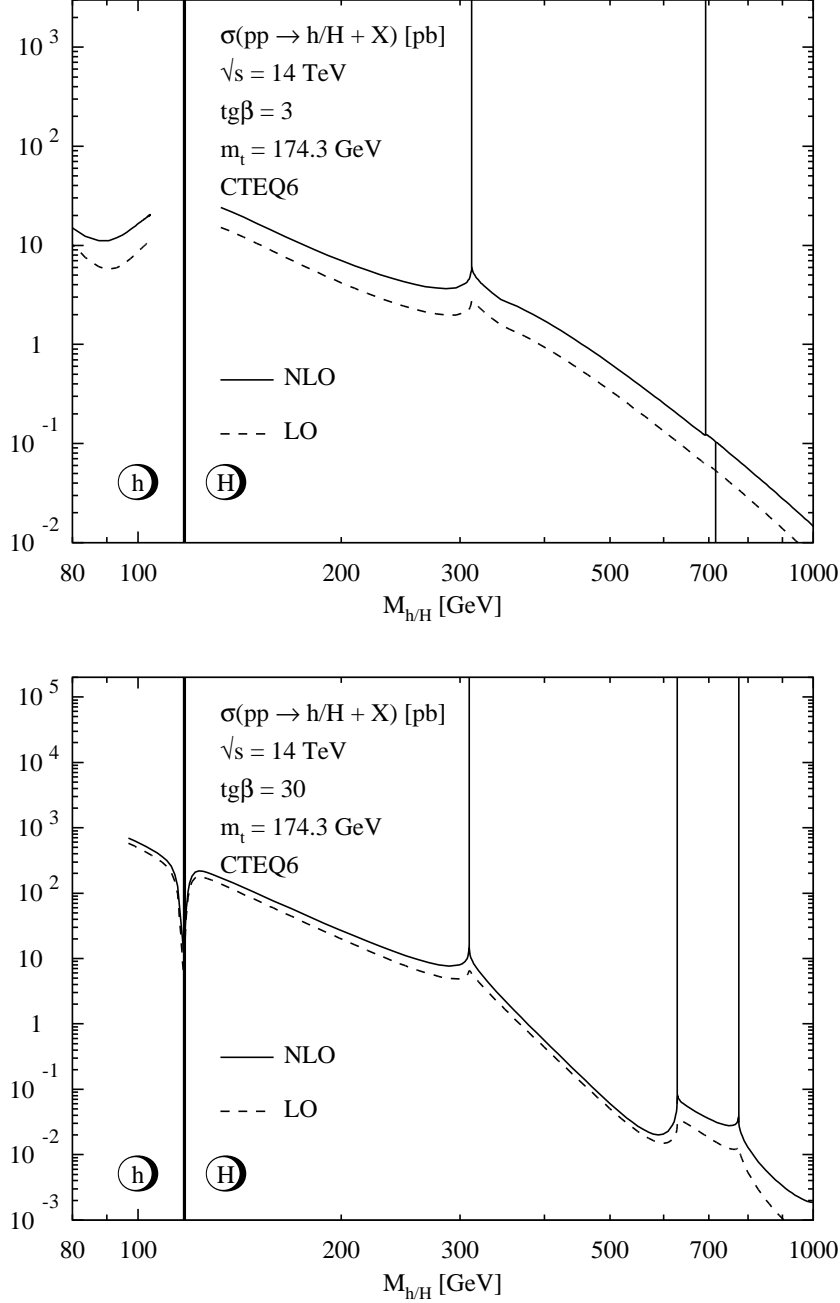


Figure 15: Production cross sections of the scalar MSSM Higgs bosons via gluon fusion as functions of the corresponding Higgs masses for $\tan\beta = 3$ and 30. The full curves include the QCD corrections, while the dashed lines correspond to the leading-order predictions. The kinks and spikes correspond to the $\tilde{t}_1\tilde{t}_1$, $\tilde{b}_1\tilde{b}_1$ and $\tilde{b}_2\tilde{b}_2$ thresholds in consecutive order with rising Higgs mass. The renormalization and factorization scales are chosen as the corresponding Higgs mass.

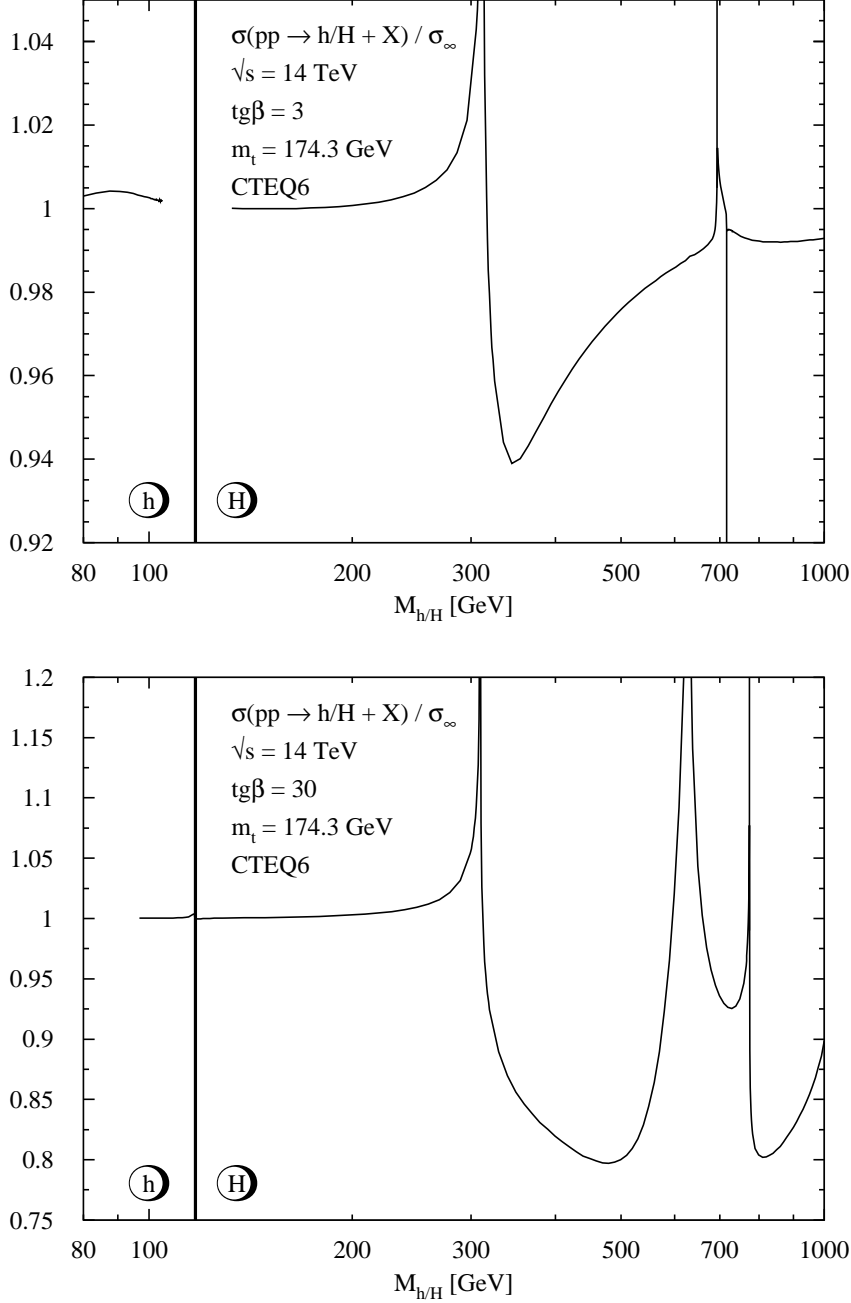


Figure 16: Ratio of the QCD corrected production cross sections of the scalar MSSM Higgs bosons via gluon fusion including the full squark mass dependence and those obtained by taking the relative QCD corrections to the squark loops in the heavy mass limit as functions of the corresponding Higgs masses for $\tan\beta = 3$ and 30. The kinks and spikes correspond to the $\tilde{t}_1\tilde{t}_1$, $\tilde{b}_1\tilde{b}_1$ and $\tilde{b}_2\tilde{b}_2$ thresholds in consecutive order with rising Higgs mass. The renormalization and factorization scales are chosen as the corresponding Higgs mass.

3 Conclusions

We have presented a NLO QCD calculation for the squark loop contributions to the production of neutral scalar MSSM Higgs bosons at the LHC and their decay modes into gluons and photons. The photonic couplings of these Higgs particles play a significant role at a future photon collider, which may be built by Compton backscattering of laser light from electron beams of a linear e^+e^- collider. The corrections stabilize the theoretical predictions compared to the LO predictions. The QCD corrections turn out to be sizeable for the photonic Higgs couplings and large for the gluonic Higgs decays as well as the gluon fusion processes. They increase the latter cross sections and gluonic decay widths significantly so that the results have to be taken into account for reliable analyses based on these processes. Despite of the large size of the NLO corrections the approximate results in the heavy top mass limits for the gluonic decay widths and gluon-fusion cross sections indicate sufficient perturbative convergence. The corrections beyond NLO are expected to be of moderate size for the central scale choices. Squark mass effects on the relative QCD corrections are sizeable and larger than the corresponding quark mass effects for the quark loop contributions. It should be noted that squark mass effects are always relevant, if the squark masses are of the order of the top mass, or the Higgs mass is larger than the corresponding virtual squark-antisquark threshold. Our results have been implemented in the program HIGLU [36] and can thus be applied to other MSSM scenarios, too.

Note added in proof. During the final write-up of our work two independent papers appeared [37], where the virtual corrections to the quark and squark loops of the gluon fusion processes $gg \rightarrow h/H$ have been derived analytically. However, a full numerical analysis of the gluon fusion processes at NLO is not contained in these papers.

Acknowledgements. We would like to thank P.M. Zerwas for valuable comments on the manuscript. M.S. would like to thank LAPTH for their very kind hospitality during his stay, where major parts of this work have been performed.

References

- [1] P.W. Higgs, Phys. Lett. **12** (64) 132; F. Englert and R. Brout, Phys. Rev. Lett. **13** (1964) 321; G.S. Guralnik, C.R. Hagen and T.W. Kibble, Phys. Rev. Lett. **13** (1964) 585.
- [2] S. Dimopoulos and H. Georgi, Nucl. Phys. **B193** (1981) 150; N. Sakai, Z. Phys. **C11** (1981) 153; K. Inoue, A. Kakuto, H. Komatsu and S. Takeshita, Prog. Theor. Phys. **67** (1982) 1889, *ibid.* **70** (1983) 330, *ibid.* **71** (1984) 413; E. Witten, Nucl. Phys. **B231** (1984) 419.
- [3] See e.g. G. Degrassi, S. Heinemeyer, W. Hollik, P. Slavich and G. Weiglein, Eur. Phys. J. **C28** (2003) 133 [arXiv:hep-ph/0212020].

- [4] M. Spira and P. M. Zerwas, arXiv:hep-ph/9803257; M. Gomez-Bock, M. Mondragon, M. Muhlleitner, R. Noriega-Papaqui, I. Pedraza, M. Spira and P. M. Zerwas, J. Phys. Conf. Ser. **18** (2005) 74 [arXiv:hep-ph/0509077].
- [5] H. Haber and G. Kane, Phys. Rep. **117** (1985) 75.
- [6] A. Djouadi, J. Kalinowski, P. Ohmann and P.M. Zerwas, Z. Phys. **C74** (1997) 93 [arXiv:hep-ph/9605339].
- [7] M. Spira, Fortsch. Phys. **46** (1998) 203 [arXiv:hep-ph/9705337]; A. Djouadi, arXiv:hep-ph/0503172 and hep-ph/0503173.
- [8] M. Spira, A. Djouadi, D. Graudenz and P.M. Zerwas, Phys. Lett. **B318** (1993) 347 and Nucl. Phys. **B453** (1995) 17.
- [9] M. Krämer, E. Laenen and M. Spira, Nucl. Phys. **B511** (1998) 523; M. Spira, arXiv:hep-ph/9703355.
- [10] A. Djouadi, M. Spira and P.M. Zerwas, Phys. Lett. **B264** (1991) 440; S. Dawson, Nucl. Phys. **B359** (1991) 283; D. Graudenz, M. Spira and P.M. Zerwas, Phys. Rev. Lett. **70** (1993) 1372; R.P. Kauffman and W. Schaffer, Phys. Rev. **D49** (1994) 551; S. Dawson and R.P. Kauffman, Phys. Rev. **D49** (1994) 2298.
- [11] R.V. Harlander and W.B. Kilgore, Phys. Rev. Lett. **88** (2002) 201801 and JHEP **0210** (2002) 017; C. Anastasiou and K. Melnikov, Nucl. Phys. **B646** (2002) 220; V. Ravindran, J. Smith and W.L. van Neerven, Nucl. Phys. **B665** (2003) 325.
- [12] S. Moch and A. Vogt, Phys. Lett. B **631** (2005) 48 [arXiv:hep-ph/0508265].
- [13] S. Dawson, A. Djouadi and M. Spira, Phys. Rev. Lett. **77** (1996) 16.
- [14] R. V. Harlander and M. Steinhauser, Phys. Lett. B **574** (2003) 258 [arXiv:hep-ph/0307346], Phys. Rev. D **68** (2003) 111701 [arXiv:hep-ph/0308210], JHEP **0409** (2004) 066 [arXiv:hep-ph/0409010]; R. V. Harlander and F. Hofmann, JHEP **0603** (2006) 050 [arXiv:hep-ph/0507041].
- [15] J. A. Aguilar-Saavedra *et al.* [ECFA/DESY LC Physics Working Group], arXiv:hep-ph/0106315.
- [16] A. Djouadi, J. Kalinowski and M. Spira, Comput. Phys. Commun. **108** (1998) 56 [arXiv:hep-ph/9704448].
- [17] T. Inami, T. Kubota and Y. Okada, Z. Phys. **C18** (1983) 69.
- [18] K.G. Chetyrkin, B.A. Kniehl and M. Steinhauser, Phys. Rev. Lett. **79** (1997) 353.
- [19] P. A. Baikov and K. G. Chetyrkin, Phys. Rev. Lett. **97** (2006) 061803 [arXiv:hep-ph/0604194].

- [20] I.F. Ginzburg, G.L. Kotkin, S.L. Panfil, V.G. Serbo and V.I. Telnov, Nucl. Inst. Meth. **219** (1984) 5.
- [21] B. Badelek *et al.* [ECFA/DESY Photon Collider Working Group], Int. J. Mod. Phys. A **19** (2004) 5097 [arXiv:hep-ex/0108012]; M. M. Mühlleitner and P. M. Zerwas, Acta Phys. Polon. B **37** (2006) 1021 [arXiv:hep-ph/0511339].
- [22] A. Djouadi, M. Spira, J. van der Bij and P.M. Zerwas, Phys. Lett. **B257** (1991) 187; A. Djouadi, M. Spira and P.M. Zerwas, Phys. Lett. **B311** (1993) 255; K. Melnikov and O. Yakovlev, Phys. Lett. **B312** (1993) 179; M. Inoue, R. Najima, T. Oka and J. Saito, Mod. Phys. Lett. **A9** (1994) 1189; M. Spira, arXiv:hep-ph/9504339.
- [23] H. Zheng and D. Wu, Phys. Rev. **D42** (1990) 3760; S. Dawson and R.P. Kauffman, Phys. Rev. **D47** (1993) 1264.
- [24] M. Steinhauser, report MPI-PHT-96-130, hep-ph/9612395, Proceedings Ringberg Workshop on “The Higgs Puzzle – What can we learn from LEP2, LHC, NLC and FMC?”, Ringberg, Germany 1996.
- [25] A. Djouadi, V. Driesen, W. Hollik and J. I. Illana, Eur. Phys. J. C **1** (1998) 149 [arXiv:hep-ph/9612362].
- [26] M. Carena, S. Heinemeyer, C. E. M. Wagner and G. Weiglein, Eur. Phys. J. C **26** (2003) 601 [arXiv:hep-ph/0202167].
- [27] J. R. Ellis, M. K. Gaillard and D. V. Nanopoulos, Nucl. Phys. B **106** (1976) 292; M. A. Shifman, A. I. Vainshtein, M. B. Voloshin and V. I. Zakharov, Sov. J. Nucl. Phys. **30** (1979) 711 [Yad. Fiz. **30** (1979) 1368].
- [28] M. M. Mühlleitner, M. Krämer, M. Spira and P. M. Zerwas, Phys. Lett. B **508** (2001) 311 [arXiv:hep-ph/0101083]; M. M. Mühlleitner, arXiv:hep-ph/0008127; D. M. Asner, J. B. Gronberg and J. F. Gunion, Phys. Rev. D **67** (2003) 035009 [arXiv:hep-ph/0110320]; P. Niezurawski, arXiv:hep-ph/0503295; P. Niezurawski, A. F. Zarnecki and M. Krawczyk, arXiv:hep-ph/0307180 and *In the Proceedings of 2005 International Linear Collider Workshop (LCWS 2005), Stanford, California, 18-22 Mar 2005, pp 0112* [arXiv:hep-ph/0507006]; M. Spira, P. Niezurawski, A. F. Zarnecki and M. Krawczyk, in preparation.
- [29] J. Fleischer, A. V. Kotikov and O. L. Veretin, Nucl. Phys. B **547** (1999) 343 [arXiv:hep-ph/9808242]; R. Harlander and P. Kant, JHEP **0512** (2005) 015 [arXiv:hep-ph/0509189].
- [30] A. Sommerfeld, *Atombau und Spektrallinien*, Vieweg, Braunschweig 1939.
- [31] M. B. Voloshin, Sov. J. Nucl. Phys. **36** (1982) 143 [Yad. Fiz. **36** (1982) 247]; V. S. Fadin and V. A. Khoze, JETP Lett. **46** (1987) 525 [Pisma Zh. Eksp. Teor. Fiz. **46** (1987) 417] and Sov. J. Nucl. Phys. **48** (1988) 309 [Yad. Fiz. **48** (1988)

- 487]; K. Melnikov, M. Spira and O. I. Yakovlev, *Z. Phys. C* **64** (1994) 401 [arXiv:hep-ph/9405301].
- [32] B. A. Kniehl and M. Spira, *Z. Phys. C* **69** (1995) 77 [arXiv:hep-ph/9505225].
- [33] H. M. Georgi, S. L. Glashow, M. E. Machacek and D. V. Nanopoulos, *Phys. Rev. Lett.* **40** (1978) 692.
- [34] R. K. Ellis, I. Hinchliffe, M. Soldate and J. J. van der Bij, *Nucl. Phys. B* **297** (1988) 221; U. Baur and E. W. N. Glover, *Nucl. Phys. B* **339** (1990) 38; O. Brein and W. Hollik, *Phys. Rev. D* **68** (2003) 095006 [arXiv:hep-ph/0305321]; U. Langenegger, M. Spira, A. Starodumov and P. Trüb, *JHEP* **0606** (2006) 035 [arXiv:hep-ph/0604156].
- [35] G. Altarelli and G. Parisi, *Nucl. Phys.* **B126** (1977) 298.
- [36] M. Spira, arXiv:hep-ph/9510347.
- [37] C. Anastasiou, S. Beerli, S. Bucherer, A. Daleo and Z. Kunszt, arXiv:hep-ph/0611236; U. Aglietti, R. Bonciani, G. Degrossi and A. Vicini, arXiv:hep-ph/0611266.